CHAPTER 4

MAGNETIC PROPERTIES OF FERRITE WOOD

4.1 Magnetic Properties of Ni-Zn ferrite wood

4.1.1 Magnetic hysteresis of Ni-Zn ferrite wood

The experiment setup for magnetic hysteresis was described at section 2.9. This purpose of this experiment is to determine either the woody shape of ferrite wood will affect the magnetism or not. The specimens were prepared in cubical shape in order to minimize or eliminated the error due to diamagnetism effect in multi-directions.

As a results, Figure 4.1 – 4.3 shows the magnetic hysteresis for all three direction for all specimens of Ni_xZn_{1-x} Fe_2O_4 (x = 0.1, 0.5 and 0.9). It seems that all specimens exhibited the similar pattern of magnetic hysteresis, which are in parallel direction (B dir) was show the higher magnetization in the lower coercive forces (Saturated at lower coercivity) compared with A and C directions.

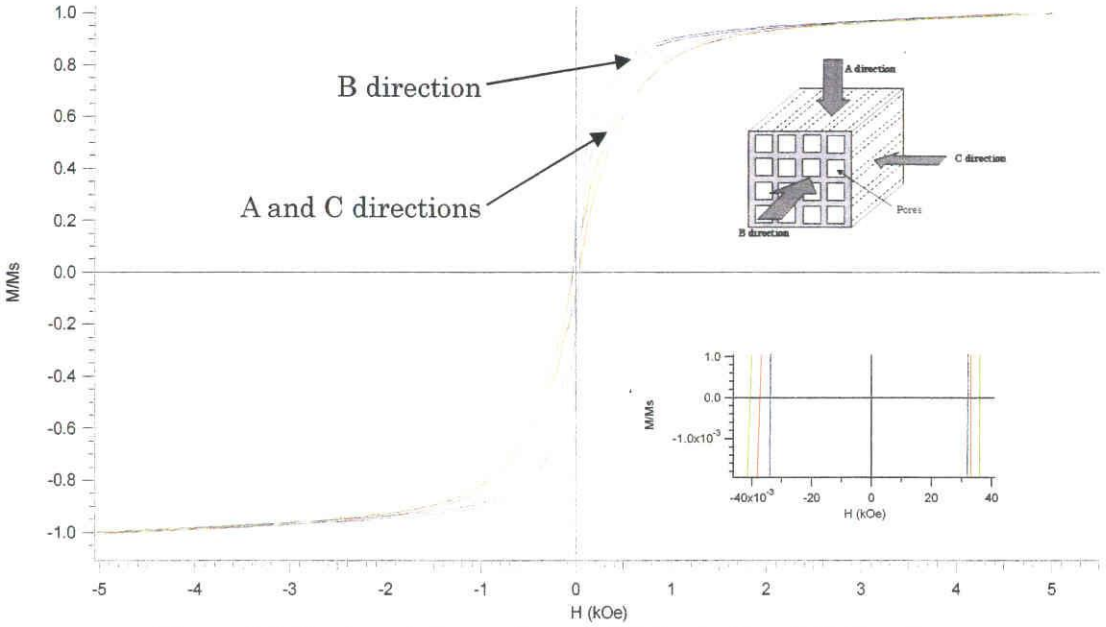

Figure 4.1 Hysteresis loops for x = 0.1 in A, B and C directions

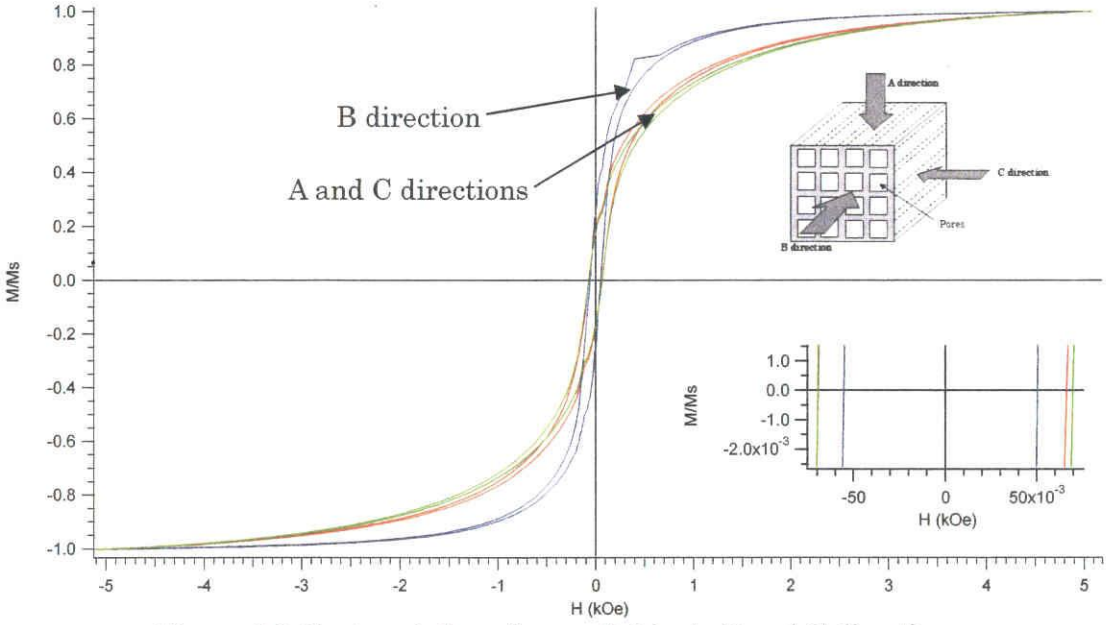

Figure 4.2 Hysteresis loop for x = 0.5 in A, B and C directions

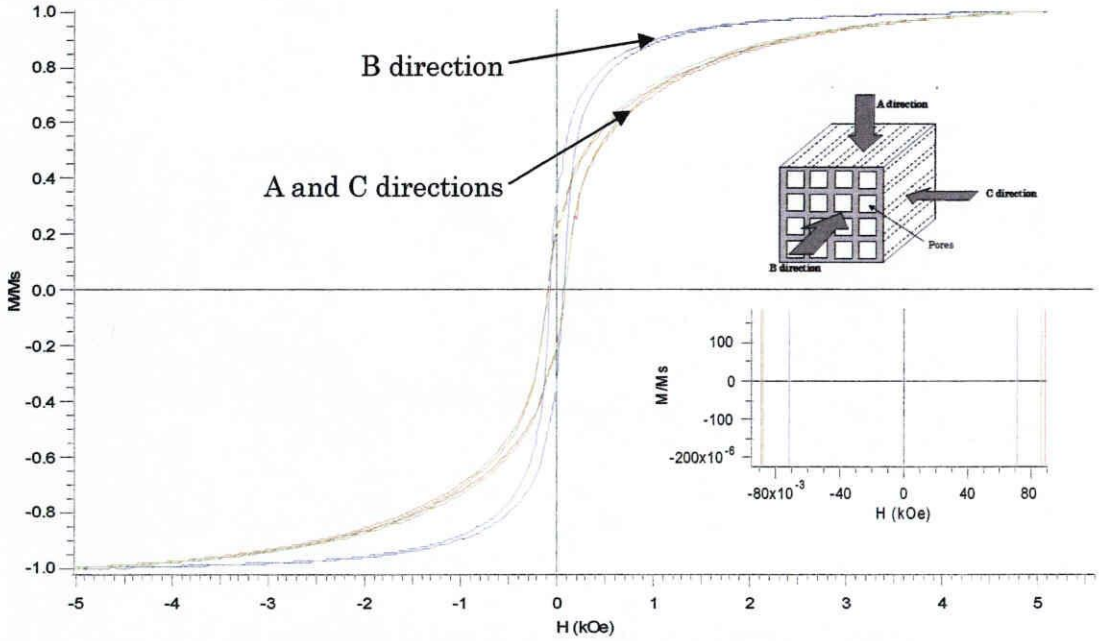

Figure 4.3 Hysteresis loop for x = 0.9 in A, B and C directions

The hysteresis curve shows that in parallel directions were easier to magnetize. The hysteresis curves Ni-Zn ferrites are have a similar trend as film shape specimens. O. F. Caltun (2005) [30] was prepared the $Ni_{0.5}Zn_{0.5}$ Fe_2O_4 film by using pulsed laser deposition technique was and mention about the typical in plane and out- of- plane magnetization curve (figure 4.4), which is similar pattern in this study.

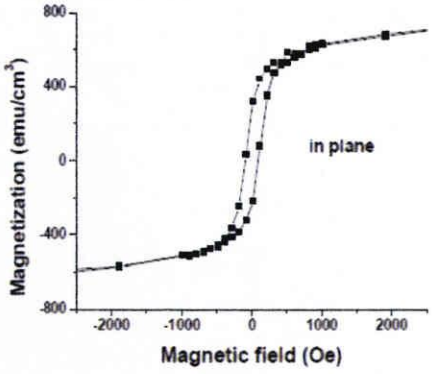

Fig. 5. VSM magnetization loops of Ni-Zn ferrite film measured in plane.

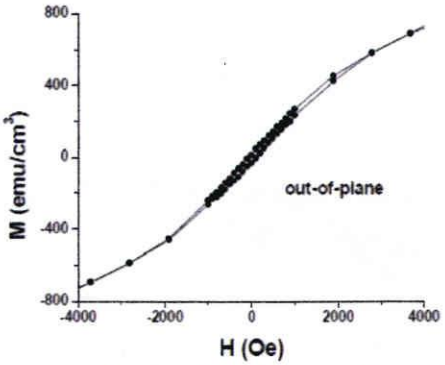

Fig. 6. VSM magnetization loops of Ni-Zn ferrite film measured out-of-plane (perpendicular to the film plane).

Figure 4.4 Magnetic hysteresis of ferrite film in plan and out-of plane. Adapted from [30]

Meanwhile for bulk ferrite [28, 41, 25] and powder ferrite [17] (non- film) most of the study only presented single hysteresis curve due to identical pattern for

every directions. The microstructure of wood that consisted layered of sintered body capable to affect the hysteresis similar pattern as film shape.

4.1.2 Characteristic of hysteresis curve of Ni-Zn ferrite wood

Two different hysteresis curves were obtained from Ni-Zn ferrite woods. Figure 4.5 and Table 4.1 indicates the characteristic of hysteresis curves that measured in perpendicular and parallel with the pores.

Table 4.1 The characteristic hysteresis curve of Ni-Zn ferrite wood

Parameter	Parallel with the pores (Doted line)		Perpendicular with the pores (Solid line)	Point (figure)
Magnetic Saturation, Ms	$\mathbf{Ms}_{pal}$	=	$\mathbf{Ms}_{per}$	
Coercivity, Hc	$\mathbf{Hc}_{pal}$	<	$\mathbf{Hc}_{per}$	
Remanence, Mr	$\mathbf{Mr}_{pal}$	>	$\mathbf{Mr}_{per}$	
Magnetization	$(\mathbf{Mr}_{pal} < \mathbf{M}_{pal} < \mathbf{Ms}_{pal})$	>	$(\mathbf{Mr}_{per} < \mathbf{M}_{per} < \mathbf{Ms}_{per})$	
Coercivity at Ms, H_{Ms}	$(\mathbf{H}_{Ms})_{pal}$	<	$(\mathbf{H}_{Ms})_{per}$	

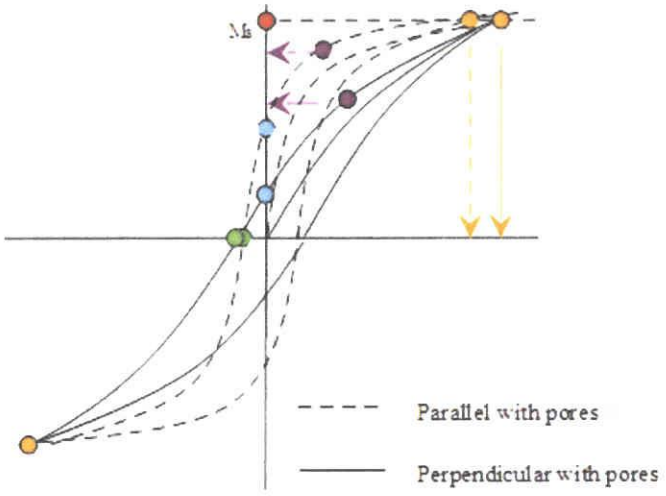

Figure 4.5 the Characteristic hysteresis curve of Ni-Zn ferrite wood

In the next following sections will discuss more detail about thus properties.

4.1.3 Coercive forces of Ni-Zn ferrite wood

Figure 4.6 show the coercive field, Hc as the function of the composition x. The coercive field, Hc increased monotonously with the increasing of x (contain of Ni^{2+}), where the coercive force in the A and C directions (perpendicular) were larger than that in the B direction (parallel to the thin wall). Therefore it is obvious that the difference of Hc in the parallel and perpendicular directions was an effect due to the anisotropic structure of wood templates. The effect also can be observed in the thin film case [42], although the coercivities Hc of thin film were much higher. The reason thin film have a higher coercivity because it have a smaller grain sizes that increase in the number of low angle grain boundaries, which acts as pinning site for domain walls [42]. Meanwhile C.Calle et al (2006) [43] were prepared the thin film by using RF sputtering and reveal that the coercivity Hc of $Ni_{0.5}Zn_{0.5}Fe_2O_4$ around ≈53 – ≈85 Oe with the thickness ≈60 - ≈240μm.

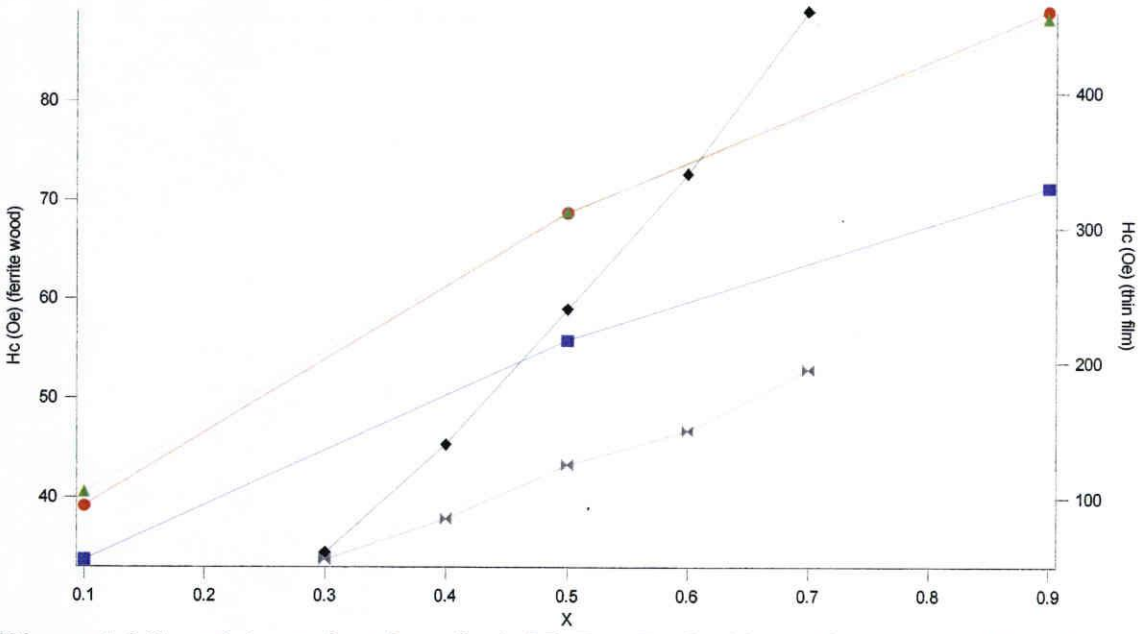

Figure 4.6 Coercivity as function of x in $Ni_xZn_{1-x}Fe_2O_4$ (a). Ferrite wood (b) Thin film [42].

The obtained results (figure 4.7) by Muhammad Ajmal et al [6] show the similar tendency of bulk ferrite prepared by solid state reaction technique are decreasing of

coercivity, Hc by increasing of Zn concentrations. The ferrite wood that consist 2 different value of coercivity due to the direction that measured in plane and off plane.

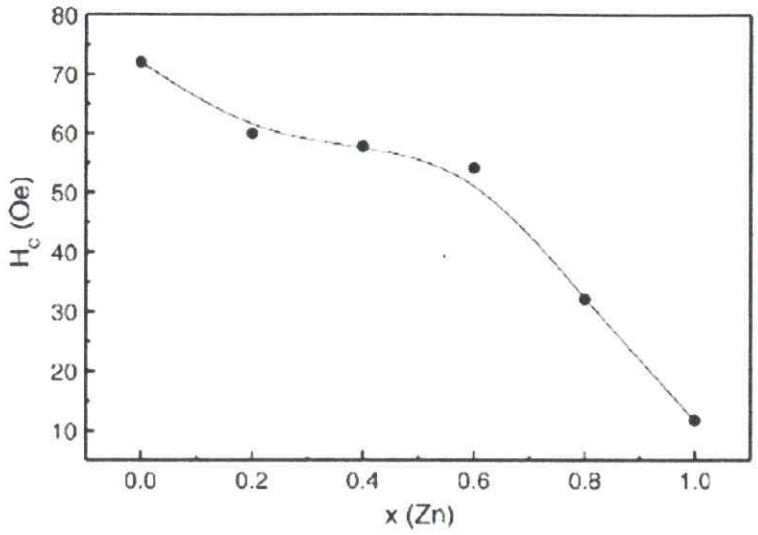

Figure 4.7 Plot of coercivity as a function of Zinc concentration in $Ni_{1-x}Zn_xFe_2O_4$. Adapted from [41]

4.1.4 Saturation of magnetization of Ni-Zn ferrite wood

For each specimen of ferrite wood (figure 4.8) was saturated at same value. Commonly, the saturation of magnetization is not directions dependent. According to J.Gao et al. (2004) [21] for the non-film $Ni_xZn_{1-x}Fe_2O_4$ have a highest magnetization saturation when x = 0.5. S.Deka et al (2006) reported that the magnetization was increased by increasing of sintering temperature from 400°C to 800°C. At 800°C the magnetization was saturated at ≈ 70 emu/g. The value of saturation was higher probably due to the small particle of powder (54 nm).

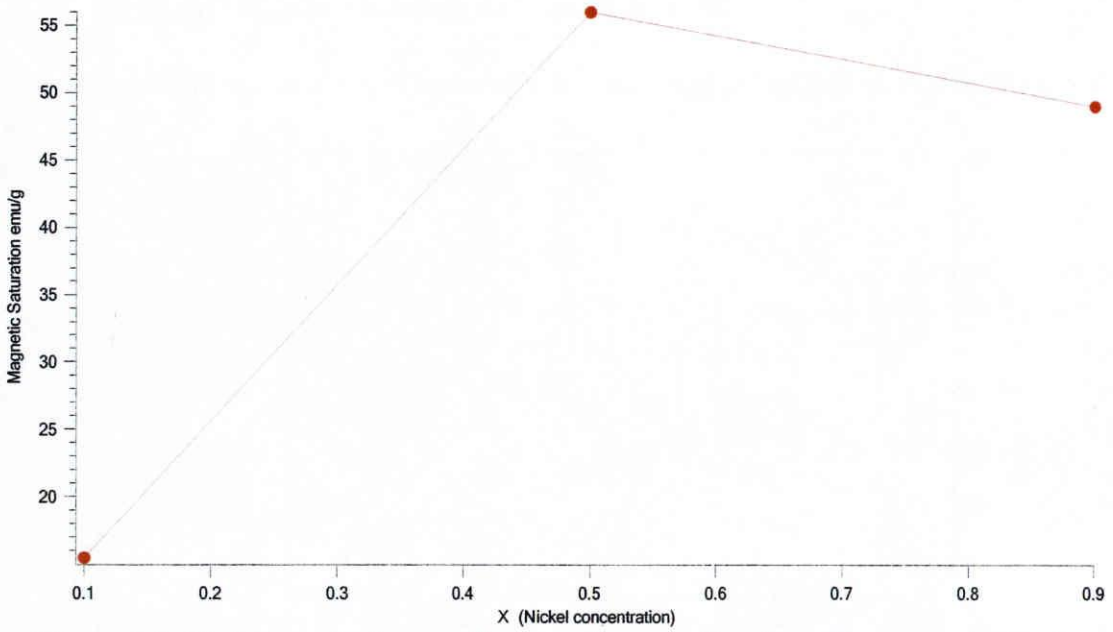

Figure 4.8. Variation of of magnetic saturation as a function of x concentration in $Ni_xZn_{1-x}Fe_2O_4$

Purushotham Yadoji at al (2003) [28], had prepared the bulk $Ni_xZn_{1-x}Fe_2O_4$ by microwave and conventional method. They were found that the saturations of magnetization are different for both processes. The results for conventional method are similar with this study. Figure 4.9 shows the results of magnetic saturations via conventional and microwave method [28]. They explain the reason the different occur because more and more Zn^{2+}occupying the tetrahedral sites by conventional technique.

The distribution of the cation in tetrahedral and octahedral will influence the magnetization in the rich Ni^{2+} region due to the net moment that produce by parallel and anti- parallel fashion. It can be explained by the equation below [44].

$$\mu_m = \{n[(1-x)-x] -5[1+(1-x)-x]\} = \{n[1-2x]-10[1-x]\}\ \mu_b$$

According to the equation above, the net moment that calculated theoretically from the Outer-shell electron configuration and number or unpaired electrons (table 4.2) was different from the experimentally obtained at higher amount of Ni^{2+}. The pattern of the normal spinel, mixed spinel and inverse spinel was increase constantly

in straight line reaching $10\mu_b$. Mean while experimentally at 40%- 50% of the contents of the Ni in the mixed spinel, the magnetization begins to drop. This is because the antiparallelism between the diminishing number of Fe_{tet} ions and the Fe_{oct} ions cannot be maintained against the increasing antiparallel interaction on the octahedral sublattices [44]. This argument was corresponded with this study.

Table 4.2 Outer-shell electron configuration and number or unpaired electrons for Ni^{2+}, Zn^{2+} and Fe^{3+}. [44]

Ion Electron	configuration	Number of Unpaired electrons
Ni^{2+}	$3d^8$	2
Zn^{2+}	$3d^{10}$	0
Fe^{3+}	$3d^5$	5

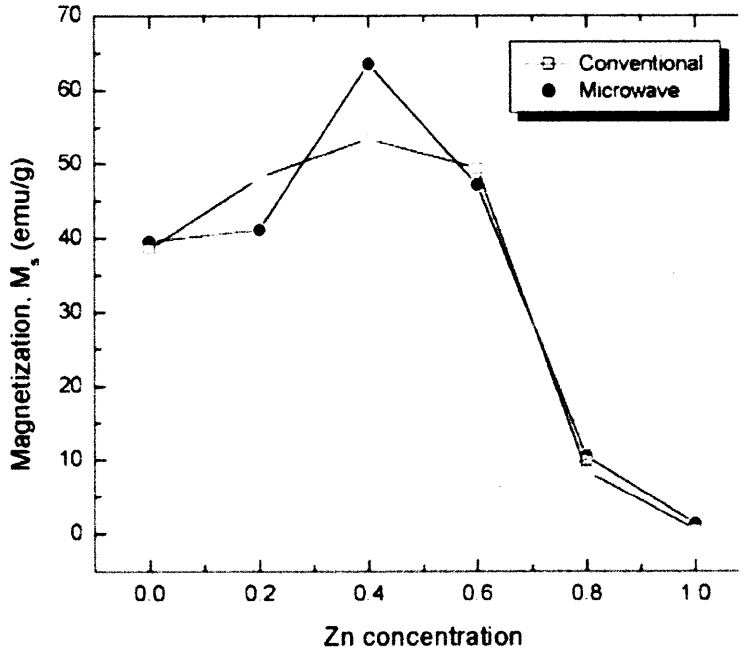

Figure 4.9 Variation of saturation magnetization with Zn concentration of $Ni_{1-x}Zn_xFe_2O_4$ (Adapted from [28])

Table 4.3 concludes the magnetic data of Ni-Zn ferrite wood.

Table 4.3 Magnetic Data of $Ni_xZn_{1-x}Fe_2O_4$ from wood templates

x	Ms		Hc (Oe)		
	Emu/g	Emu/cc	A dir	B dir	C dir
0.1	15.5	9.86	39.1	33.7	40.5
0.5	56	38.12	68.7	55.8	68.8
0.9	49	44.35	89	71	88

4.1.5 Anisotropy constant of Ni-Zn ferrite wood

The anisotropy constants were calculated by brown's relations [45]

$$H_c \geq \left(\frac{2K_1}{\mu_o M_s} \right)$$

Here we can see that the coercivity, H_c has a direct relation with the anisotropy constants K_1. In this study the coercivities were increase by increasing of Zn^{2+} and higher in perpendicular directions. For bulk spinel Ni ferrite and Mn ferrite have a K_1 = -69 x 10^{-3} and 40 x 10^{-3} erg/cm^3 respectively [44] meanwhile for ferrite wood was stated in table below.

Table 4.4 The anisotropy constant of $Ni_xZn_{1-x}Fe_2O_4$ in parallel and perpendicular dir.

X	direction to the pores	Anisotropy constant erg/cm^3
0.1	Parallel	- 3 x 10^{-3}
	Perpendicular	- 2.6 x 10^{-3}
0.5	Parallel	- 20.7 x 10^{-3}
	Perpendicular	- 16.8 x 10^{-3}
0.9	Parallel	- 31.1 x 10^{-3}
	Perpendicular	- 24.9 x 10^{-3}

The anisotropy constants were higher in parallel directions for every specimen.

4.1.6 Saturation magnetization ratio (Squareness) of Ni-Zn ferrite wood

For soft ferrite, higher the hysteresis slope, the higher the squareness. The squareness of $Ni_xZ_{1-x}Fe_2O_4$ wood in parallel and perpendicular are shown in figure 4.10.

The squareness was calculated in %. In parallel direction the squareness is higher than that in perpendicular directions. It seem like all the specimens have a different of the squareness at average 10% for both directions. The results also shows the squreness are increasing monotonously by the content of Ni^{2+}.

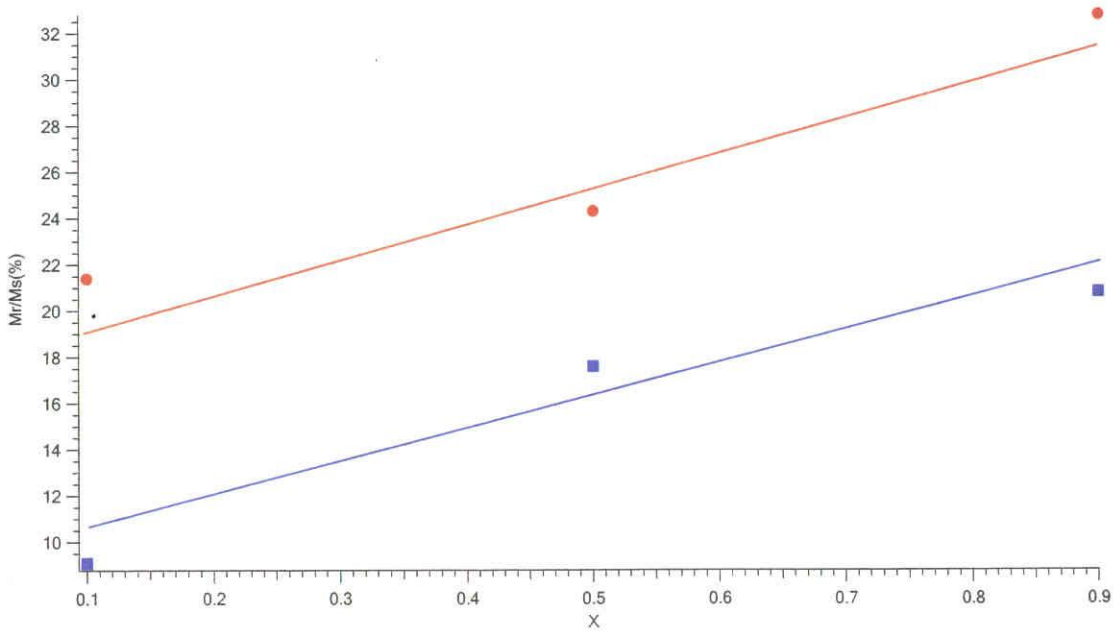

Figure 4.10 Saturation Magnetization ration (Squareness), Mr/Ms in function of X

4.1.7 Magnetic Permeability, μ of Ni-Zn ferrite wood

Magnetic permeability is the measure of the ability of a material to support the formation of a magnetic field within itself. In order to dealing with high frequency magnetic field, the complex permeability is a useful tool. The complex permeability can be explained by equation below.

$$\mu(f) = \mu'(f) - j\mu''(f)$$

Which is μ = complex permeability, μ' = real permeability and μ"= imaginary permeability. In the other word, the μ is a resultant of μ' and μ" (figure).

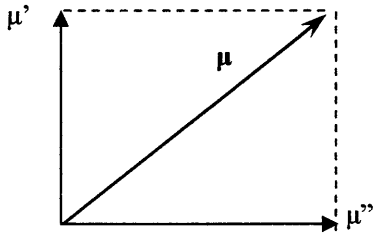

and solving for μ

$$\mu = \sqrt{((\mu')^2+(\mu'')^2)}$$

In permeability also can be determined from the magnetic hysteresis that measured by magnetization, B vs coercive force, H.

$$\mu = B/H$$

The magnetic permeability, μ is a slope of B-H curve. Which is the larger the slope the higher the permeability. From the magnetic hysteresis of ferrite wood were reveals the shape anisotropy due to the layer of wall that parallel with the pores (section 3.8.1). It was easier to magnetize if measured parallel with the pores (with 10% different of squareness). Means that it has a different slop of B-H curves that show by equation below.

$$\mu_1 = (B/H)_{\text{parallel to the pores}} \text{ and}$$

$$\mu_2 = (B/H)_{\text{perpendicular to the pores}}$$

According to those equations, two permeability might be obtained with 1 ferrite wood specimens. The next section will discuss about the dual permeability in single ferrite wood.

4.1.8 Experimental of dual permeability in single ferrite wood specimen.

Section 2.16 was discussed about the magnetic permeability measurement. Most of the equipment for high frequency (>1MHz) magnetic permeability measurement only measure the smaller size specimens that in film (max thickness 1mm) and toroidal shape. Ferrite wood was constructed by a multi- layer of wall in 1 directional pores with a size of pore approximately 10μm. That means for 1 mm thickness it consist approximately 100 layers of wall.

The value of magnetization and the H_k magnetic from hysteresis curve is necessary for the permeability measurement. The results in figure 3.31 indicate the anisotropy caused by the wall of ferrite wood also occurred in the 1mm thick specimens. As results, the value of the Magnetization and the anisotropic magnetic field strength Hk were different for each direction. The ferrite wood that sintered at 1200°C, 1250°C and 1300°C was measure (figure 4.11-4.13).

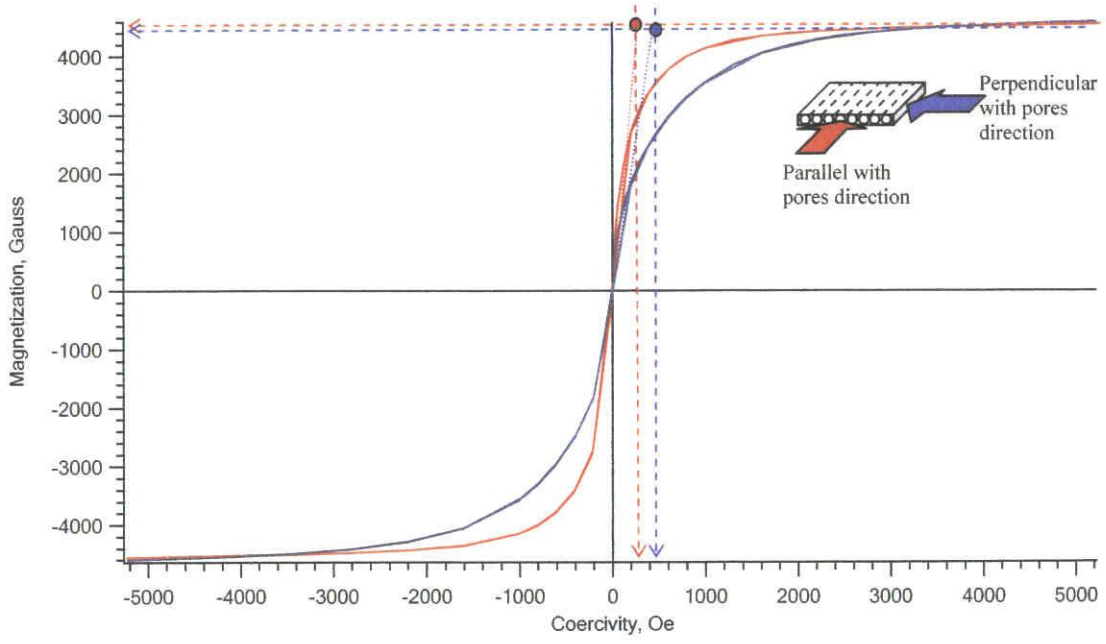

Figure 4.11 Magnetization and H_k for $Ni_{0.5}Zn_{0.5}Fe_2O_4$ (sintered at 1200°C) thin shape specimens 1.

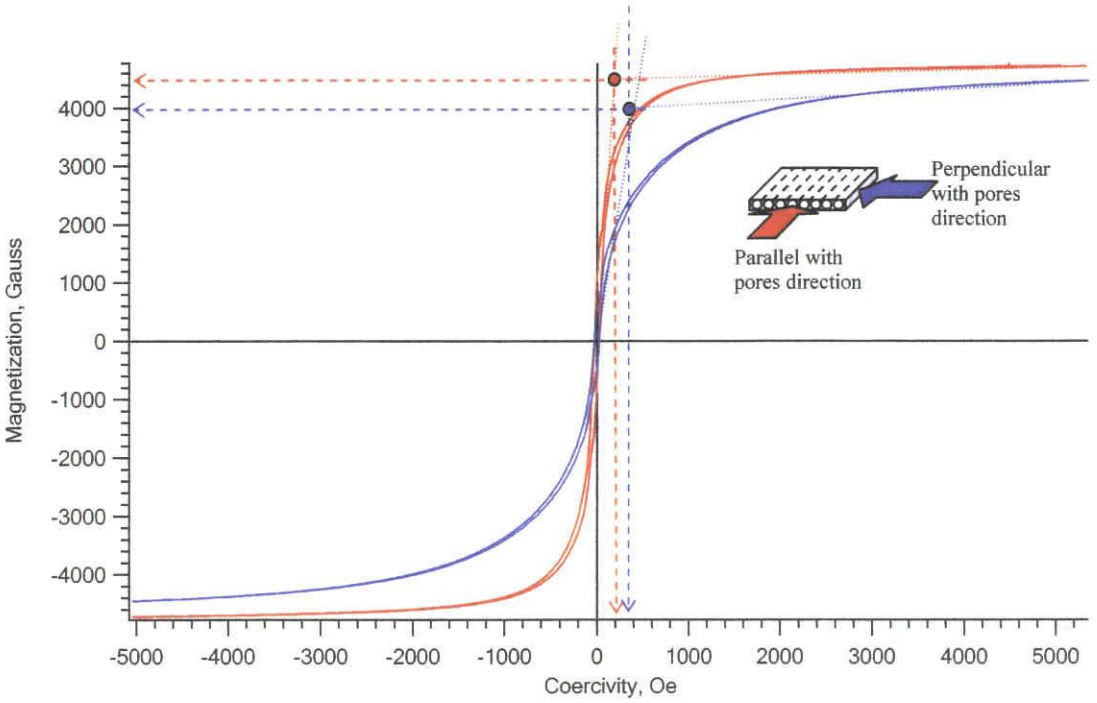

Figure 4.12 Magnetization and H_k for $Ni_{0.5}Zn_{0.5}Fe_2O_4$ (sintered at 1250°C) thin shape specimens 2.

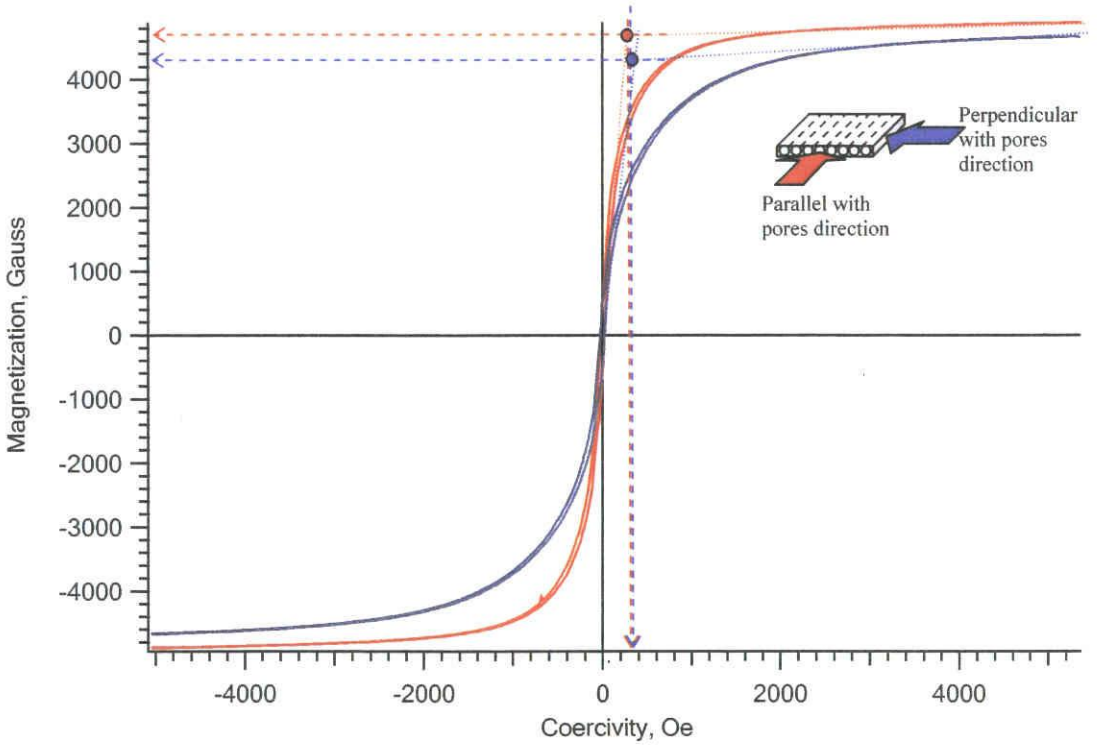

Figure 4.13 Magnetization and H_k for $Ni_{0.5}Zn_{0.5}Fe_2O_4$ (sintered at 1300°C) thin shape specimens 3.

Table 4.5 shows the input data that necessary for the permeability measurement. Each set of data shows the similar trend which is in parallel with pores

direction the value of magnetizations were higher and anisotropic magnetic field strength Hk were lower.

Table 4.5 Results obtained from hysteresis curve of ferrite wood for magnetic permeability measurement

Specimen	size (mm^3)	Directions	magnetization $4\pi Ms(kG)$	Hk (kOe)
1	1 x 5 x 6	Parallel	4.4	0.333
(1200°C)		Perpendicular	4.35	0.461
2	1 x 5 x 6	Parallel	4.5	0.205
(1250°C)		Perpendicular	4.0	0.350
3	1 x 5 x 6	Parallel	4.7	0.300
(1300°C)		Perpendicular	4.3	0.340

The ferrite woods have porosity as high as 87% caused the magnetic permeabilities were very low due to the equipment was include the air permeability of the specimens during measurement. To consider the only the sintered body, the obtained value of permeability was corrected by eliminated the pores effect.

The Permeability affected by density was eliminated by using formula

$$\mu=\mu_{exp}/(1-V_{pi})$$

in order to examined the effect of microstructure [46, 47]. V_{pi} is the volume fraction occupied by pores that can be achieved through various methods such as X-ray, microscopic analysis or the density of material [46]. For this study, the density of material method was used which is $V_{pi} = 1 - \rho_{bulk}/\rho_{theoretical}$, where ρ_{bulk} and $\rho_{theoretical}$ is the bulk density and theoretical density of the specimen respectively.

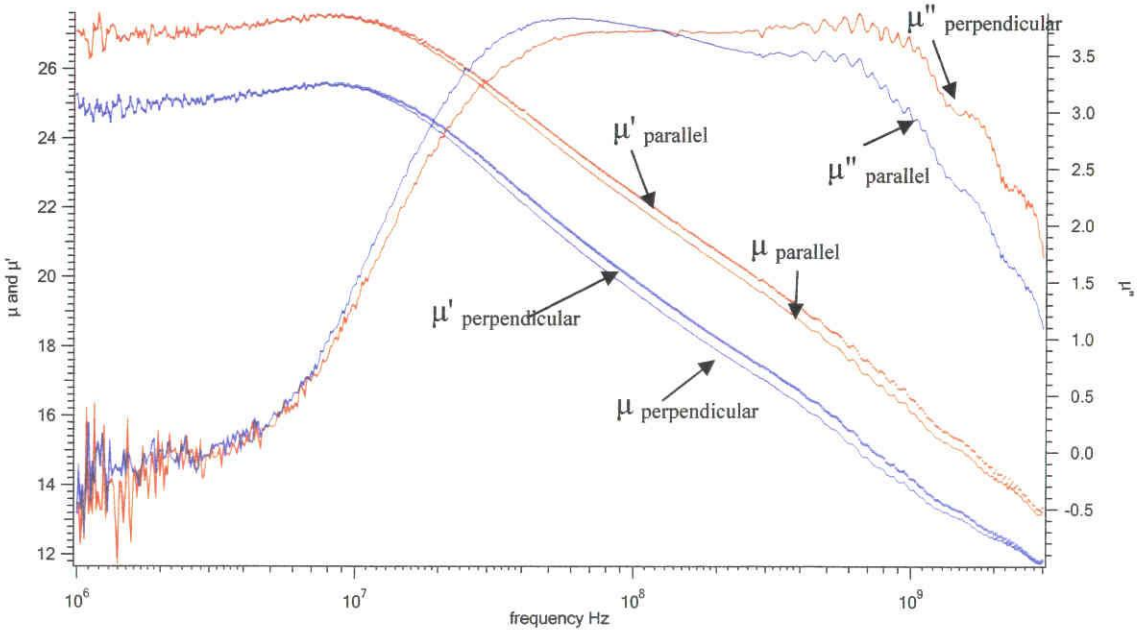

Figure 4.14 Complex permeability of ferrite wood (1200°C) in parallel and perpendicular directions.

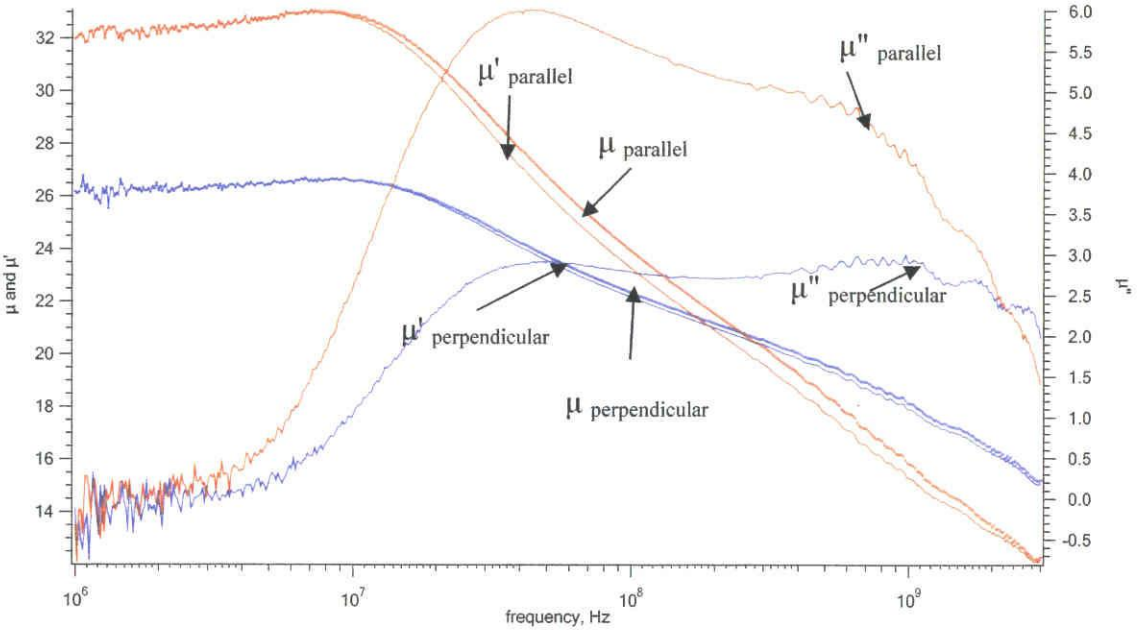

Figure 4.15 Complex permeability of ferrite wood (1250°C) in parallel and perpendicular directions.

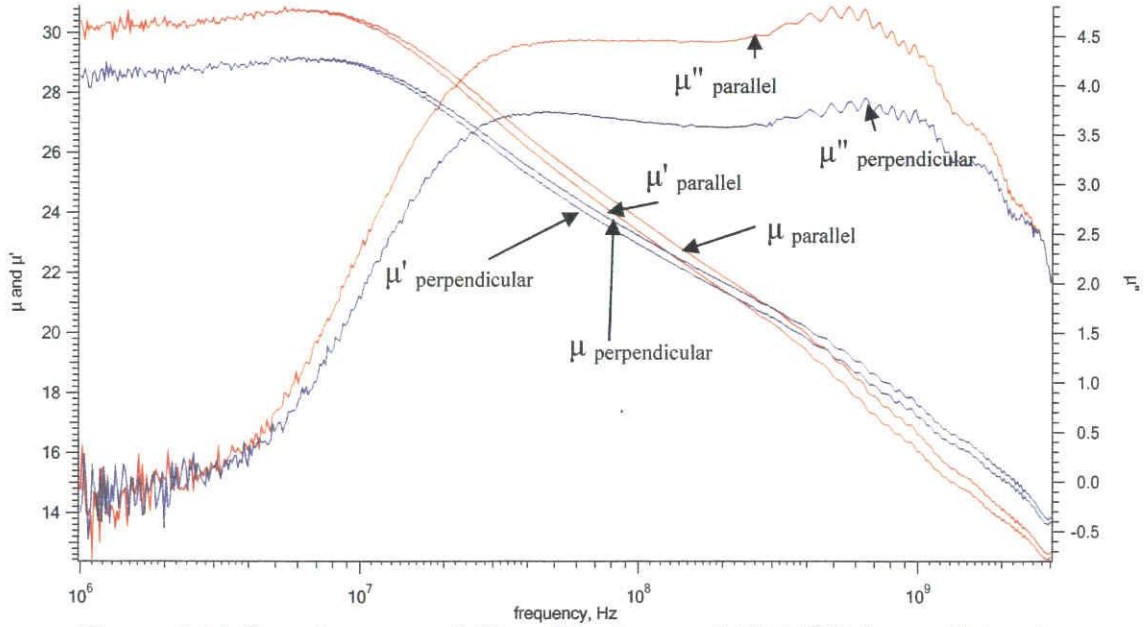

Figure 4.16 Complex permeability of ferrite wood (1300°C) in parallel and perpendicular directions.

The results were shown in figure 4.14 – 4.16. The tendencies of the magnetic permeability are similar, which is higher in parallel directions but the range of the different in parallel and perpendicular were various due to the microstructure that in-homogeneous. The imaginary permeability μ" have a multiple peak due to the inhomogeneous of the microstructure and porosity. In this study, No specific trend of the sintered temperature causing the magnetic permeability.

The results agree with the equations $\mu_1 = (B/H)_{\text{parallel to the pores}}$ and $\mu_2 = (B/H)_{\text{perpendicular to the pores}}$ that obtained via VSM measurement. This study had revealed a dual magnetic permeability in single ferrite wood caused by it microstructure.

Two main factors that contribute to the changes of the complex permeabilities namely, compositions contain of x for ($Ni_xZn_{1-x}Fe_2O_4$) figure 4.17 and the densities change. But it was related with the high density specimens. The permeability was shifted down and the peak was shifted to the higher frequency for the lower density

specimens. The density was caused by the porosity. That means for porous Ni-Zn ferrite material the peak was shifted to the higher frequency.

Figure 4.17 shows the complex permeability vs frequency with various sets of density of bulk $Ni_{0.5}Zn_{0.5}Fe_2O_4$. This results agreed with [16] that phenomenon occurred at Ni-ferrite was also similar with bulk $Ni_{0.5}Zn_{0.5}Fe_2O_4$. The results also indicate for bulk $Ni_{0.5}Zn_{0.5}Fe_2O_4$ at ~ 2GHz, the real permeability was showed the diamagnetism behavior which is lower than that air permeability, < 1. The dispersion frequency drops continuously with increasing density [16]. According to [16] this phenomenon occurred because for low density and smaller grains specimens, only domain rotations contribute to permeability and that in denser specimens a contribution is also made by wall displacements.

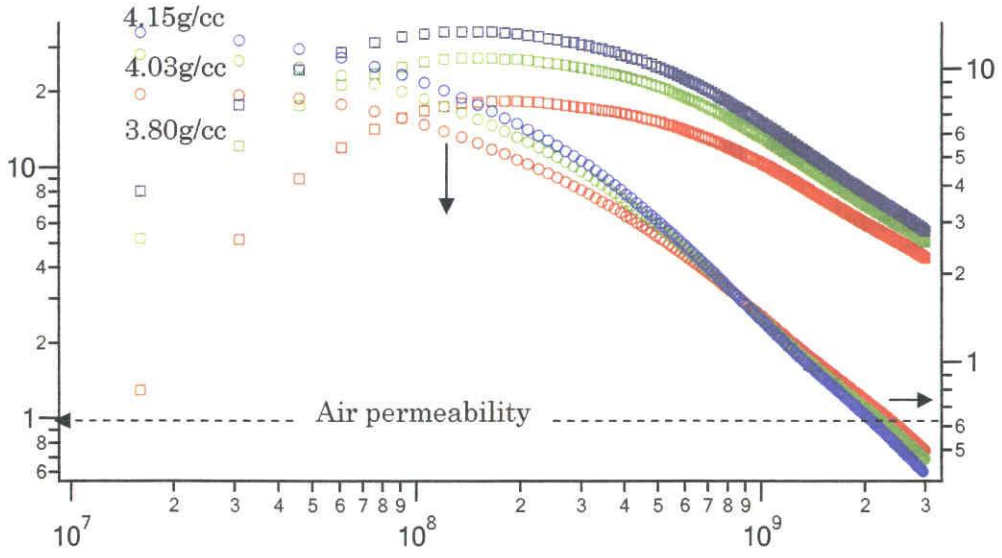

Figure 4.17 The permeability of the higher density of bulk $Ni_{0.5}Zn_{0.5}Fe_2O_4$

4.1.9 High density vs low density $Ni_{0.5}Zn_{0.5}Fe_2O_4$ at GHz frequency.

Before proceed with the results, let refresh back at the microstructure. Figure 4.18 shows the SEM images of the High Density, Low Density and ferrite wood that sintered at 1200°C. All specimens subjected with similar grain sizes at same sintering

temperature. The high density ferrite was prepared by using the calcined infiltrated wood that crushed into powder and compressed and finally sintered at desired temperature. Meanwhile for low density ferrite was prepared by the similar approach only different with additional of organic powder that mixed in order to produce the pores. As results of the preparations, all the specimens have a similar grain sizes (figure 4.18).

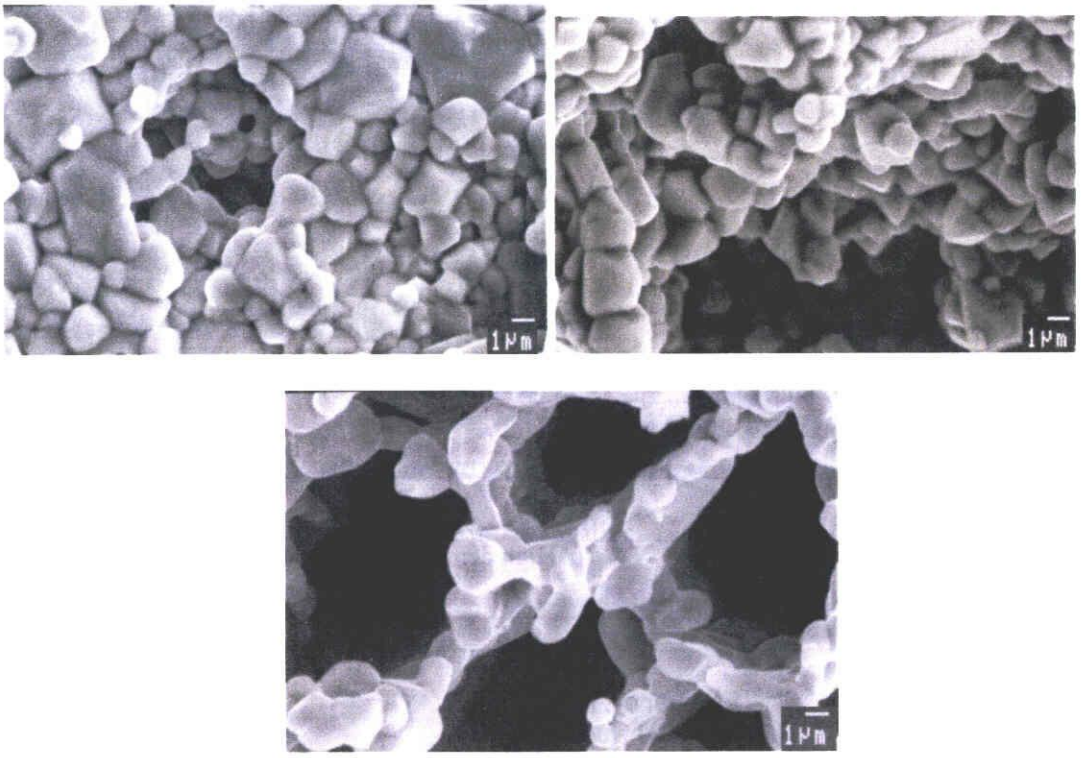

Figure 4.18 SEM images of a. High density (3.80g/cc), b. low density (~0.67g/cc) and c. ferrite wood (minimum ~0.66g/cc)

In previous section, discuss about the higher density ferrite that have diamagnetism behaviors at 1~2 GHz. The very lower density $Ni_{0.5}Zn_{0.5}Fe_2O_4$ was compared in this sections. The low density ferrite specimens (~0.6g/cc) were produced. The comparison shows that for low density ferrite has a better permeability at GHz frequency. It was agreed that the lower density $Ni_{0.5}Zn_{0.5}Fe_2O_4$ have a lower maximum permeability, but in the range 2 – 3 GHz the permeability performed ferrimagnetism behavior (permeability higher than air permeability) (figure 4.19)

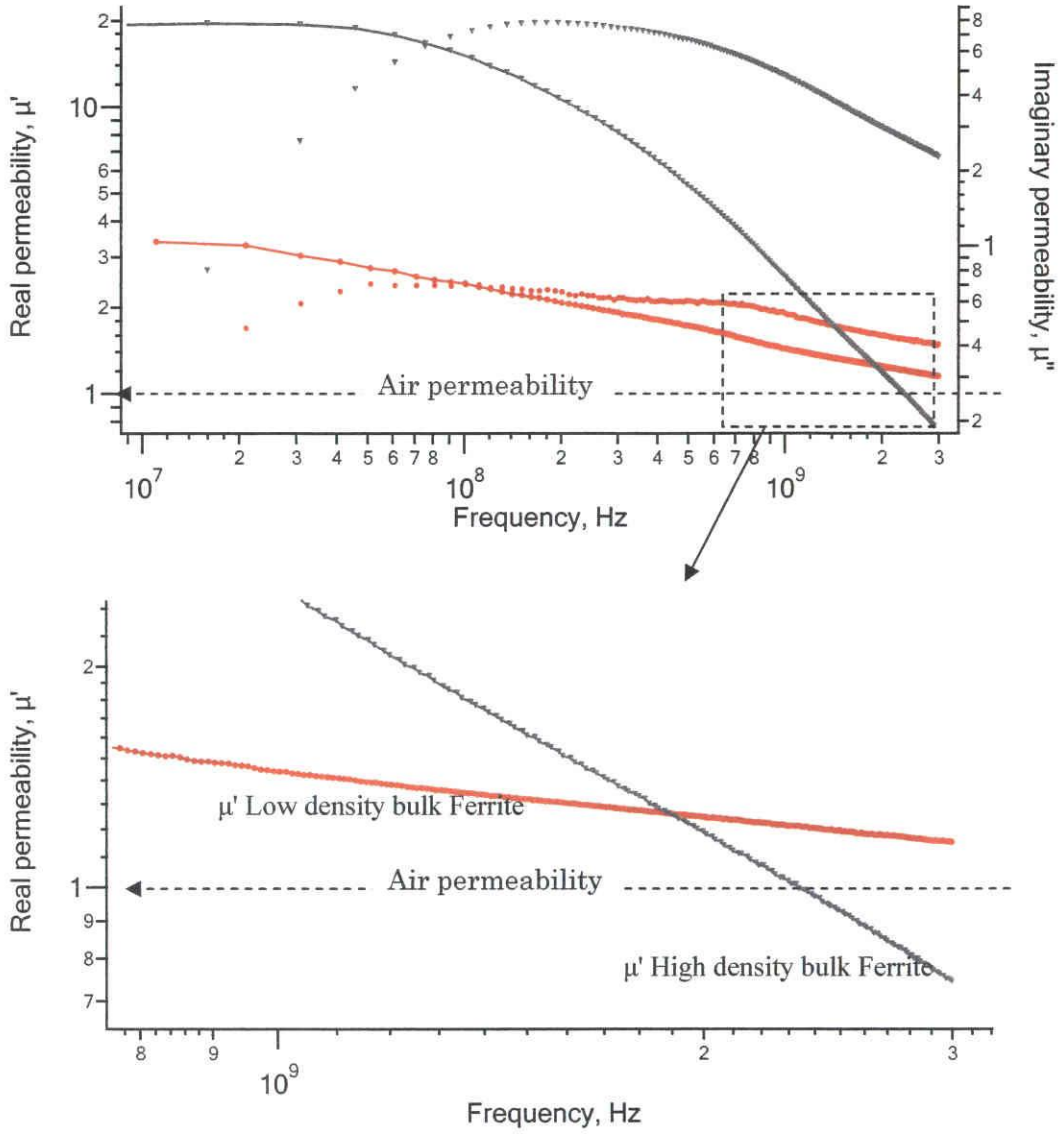

Figure 4.19 The permeability of the higher density of bulk vs low density of bulk $Ni_{0.5}Zn_{0.5}Fe_2O_4$

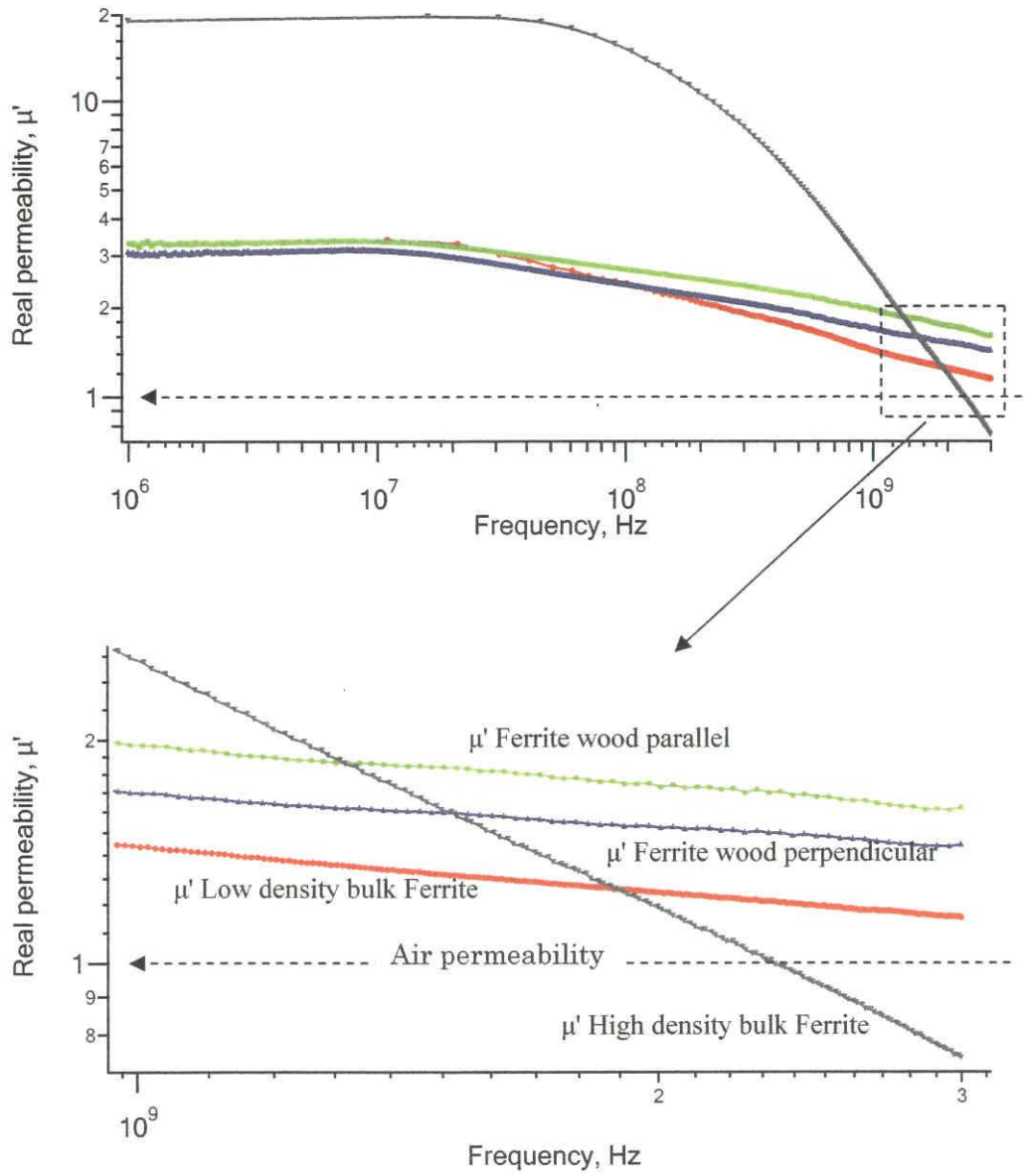

Figure 4.20 The permeability of the $Ni_{0.5}Zn_{0.5}Fe_2O_4$ wood and high porosity random pores specimens (sintered at 1200°C)

Figure 4.20 shows the permeability curve of High density ferrite, low density ferrite and ferrite wood. The low density ferrites have a similar density with ferrite wood hath sintered at 1200°C. It seem like the woody shape specimens have a better performance at GHz regions. At 3 GHz the ferrite wood have a relative real permeability at 1.6 and 1.42 compared with non-wood that slightly higher than air permeability 1.15. That means the wood microstructure capable to influence the better permeability at high frequency. This is because the shape anisotropy able to increase

the ferrimagnetic resonance frequency. as discussed earlier the high density have a diamagnetism behavior which is gave the relative real permeability lower than 1.

The results were confirmed with the specimens with different sintering temperatures. Figure 4.21 shows the specimens that sintered at 1250°C. In this case the non-wood ferrite has a similar pattern with ferrite wood that in parallel directions. Meanwhile ferrite wood that measured perpendicular with the pores have a better relative real permeability at 3GHz. Ferrite wood that measured parallel with the pores have a higher max permeability than that in perpendicular direction but after exceeded 100MHz the opposite phenomenon occurred. According to an expert, the phenomenon was due to the inhomogenity of the microstructure. These are significant due to the defected wood at higher sintering temperature. The similar pattern of curve was revealed for higher ferrite wood that sintered at 1300°C (figure 4.42).

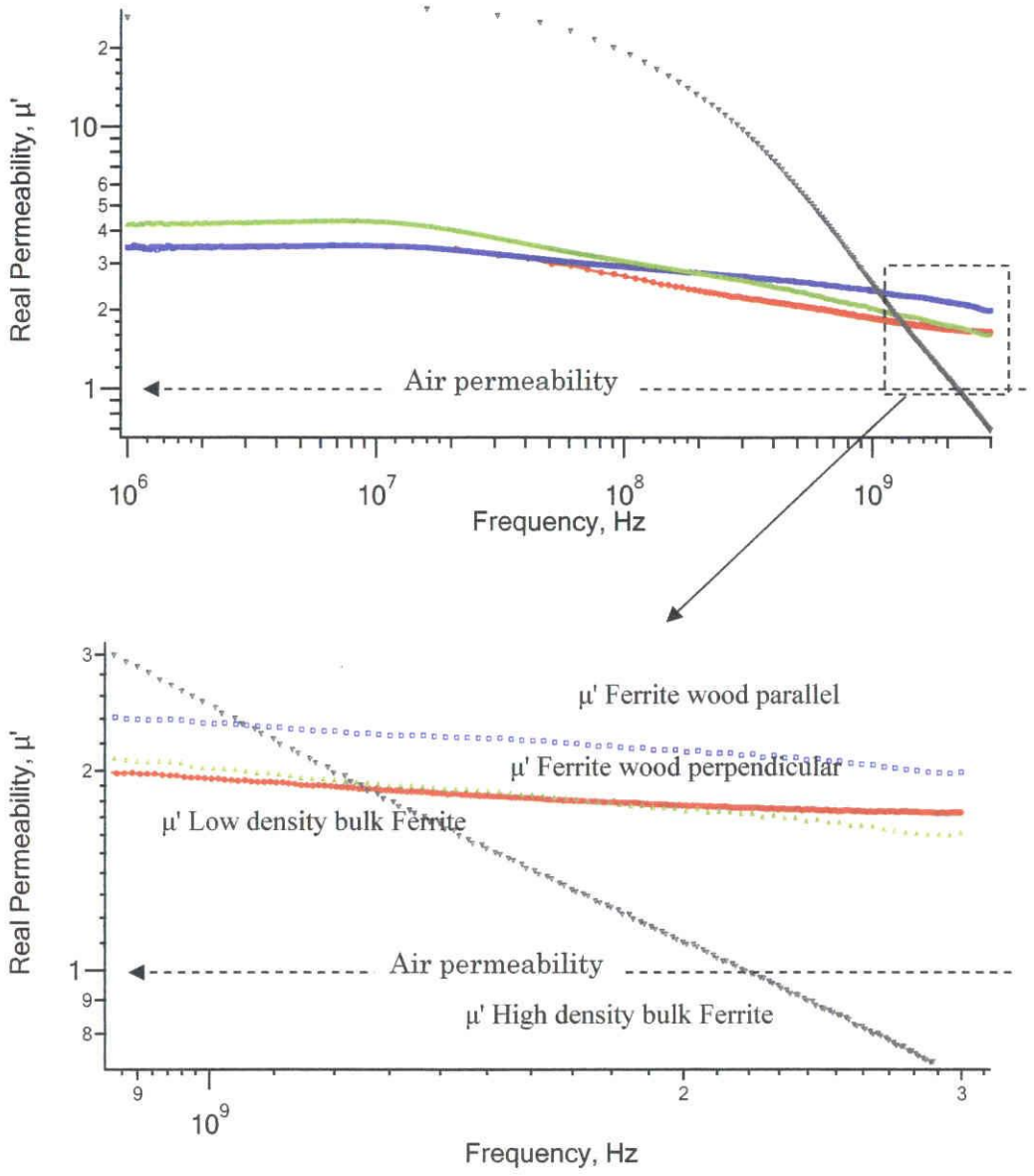

Figure 4.21 The permeability of the $Ni_{0.5}Zn_{0.5}Fe_2O_4$ wood and high porosity random pores specimens (sintered at 1250°C)

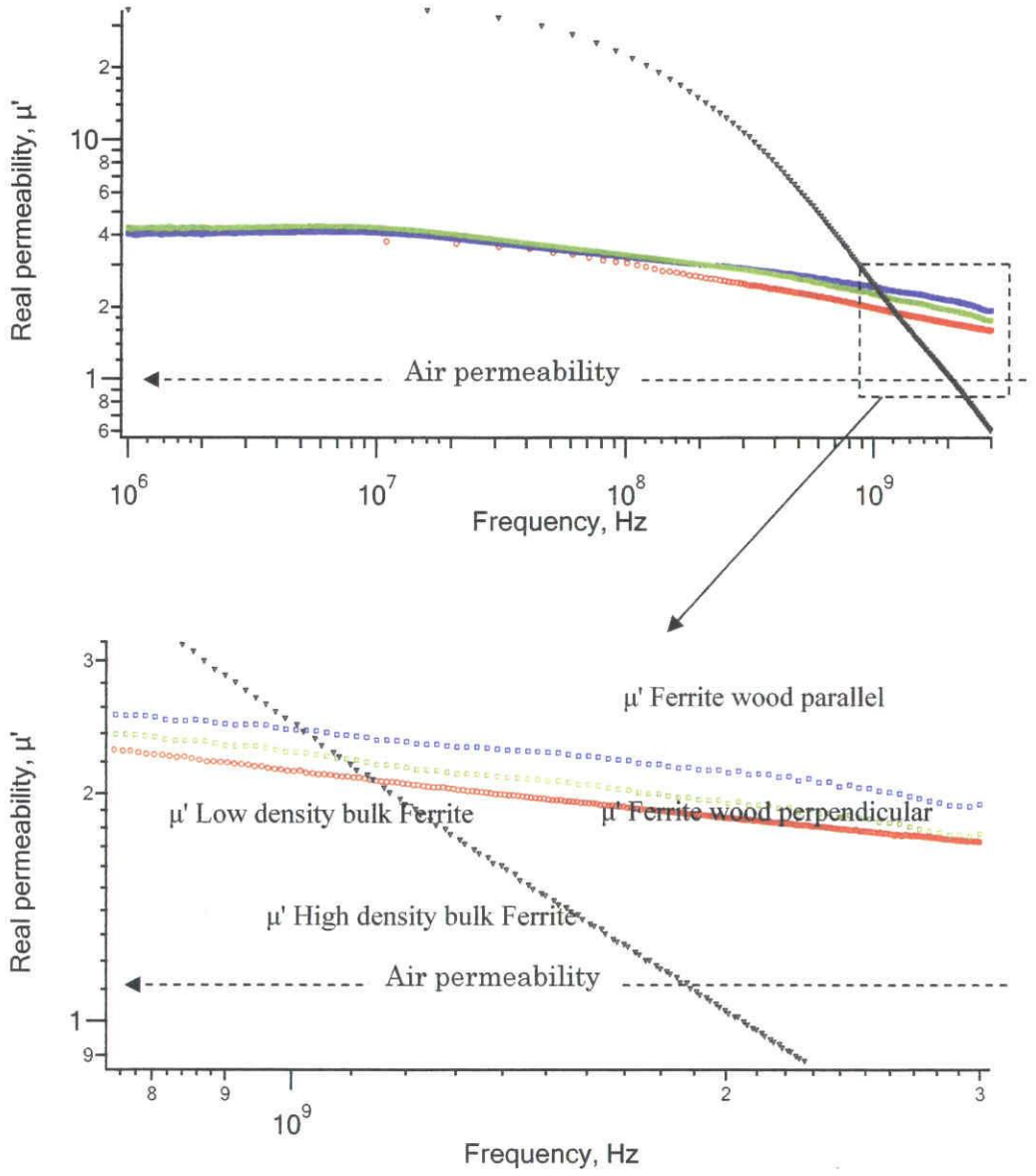

Figure 4.22 The permeability of the $Ni_{0.5}Zn_{0.5}Fe_2O_4$ wood and high porosity random pores specimens (sintered at 1300°C)

4.2 Magnetic properties of Mn-Zn ferrite wood

4.2.1 Magnetic hysteresis of Mn-Zn ferrite wood

The magnetic hystereses of cubical shape Mn-Zn ferrites wood were measured. The experiments setup was discussed in sections. The results of magnetic hysteresis of $Mn_xZn_{1-x}Fe_2O_4$ wood (x = 0.1, 0.5 and 0.9) are shown in figure 4.23 – 4.25.

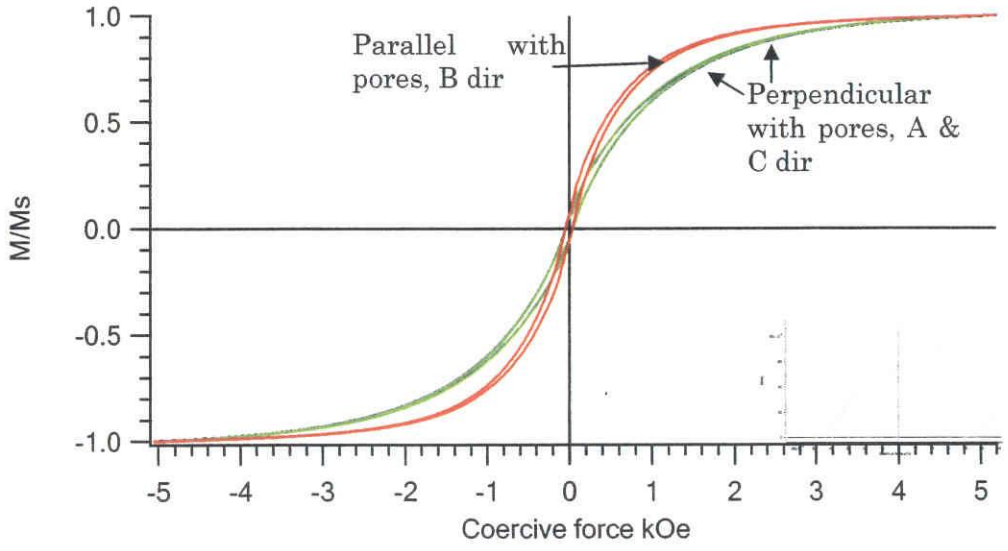

Figure 4.23 Hysteresis loop of $Mn_xZn_{1-x}Fe_2O_4$ for x = 0.1 in A, B and C directions

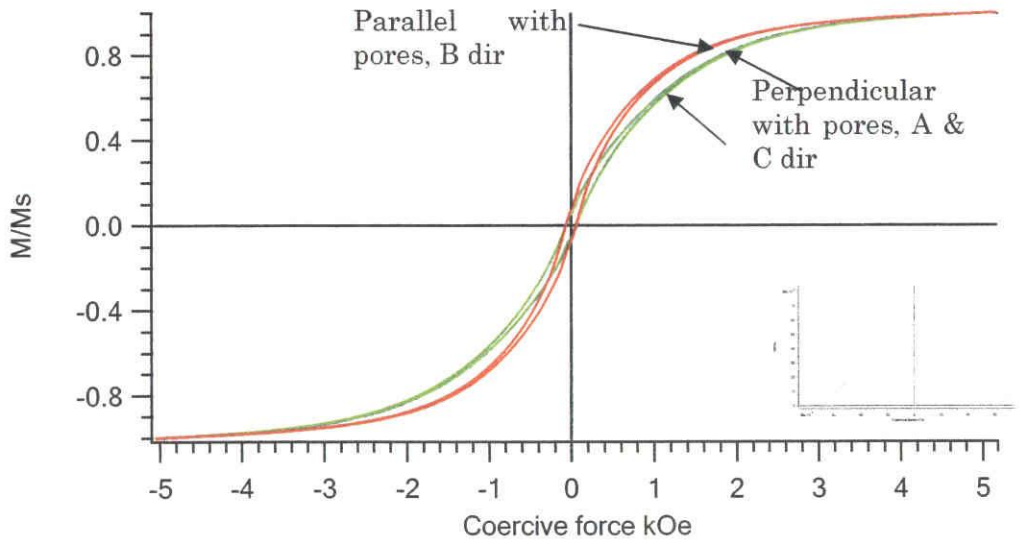

Figure 4.24 Hysteresis loop of $Mn_xZn_{1-x}Fe_2O_4$ for x = 0.5 in A, B and C directions

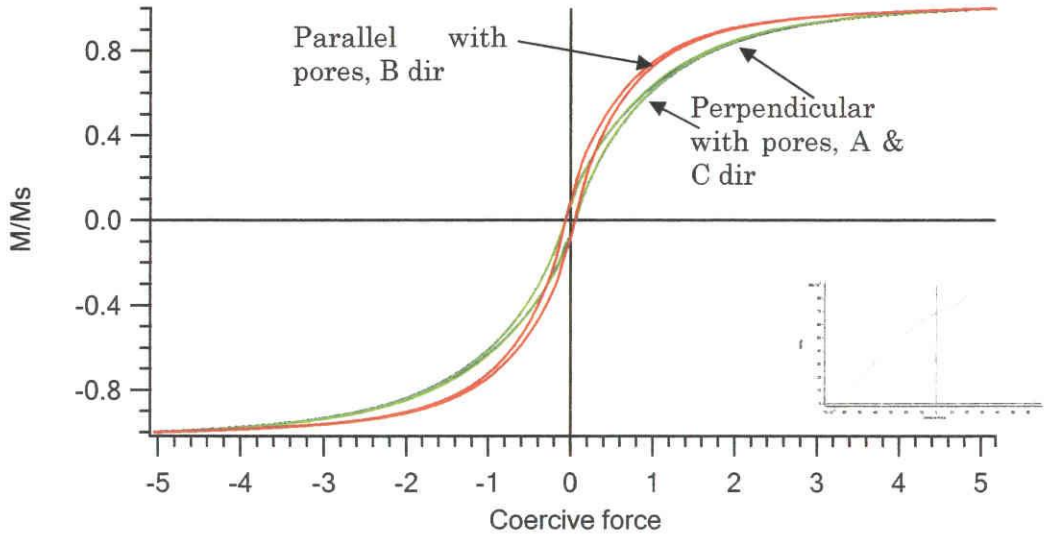

Figure 4.25 Hysteresis loop of $Mn_xZn_{1-x}Fe_2O_4$ for x = 0.9 in A, B and C directions

Instead of Ni-Zn ferrite the same tendency was occurred in Mn-Zn ferrite. The shape anisotropy was occurred at all concentrations of Mn^{2+}. The hysteresis curve of Mn-Zn ferrite wood shows the same tendency film shape specimens as reported by R.G. Welch et al (1996) (figure 4.26) that prepared Mn-Zn ferrite film by pulsed laser depositions.

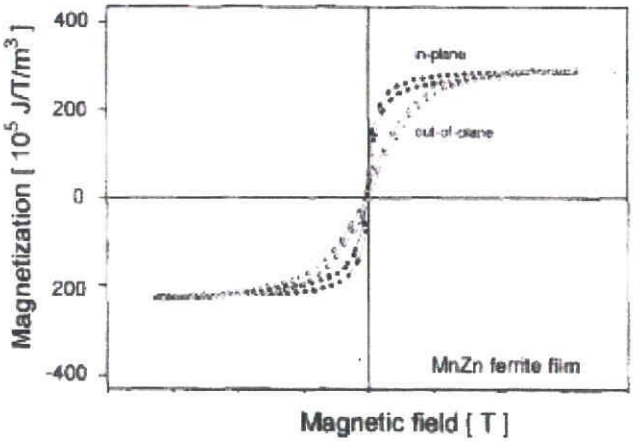

Fig. 6. VSM magnetization loops of MnZn ferrite films measured in-plane and out-of-plane.

Figure 4.26 The hysteresis loop of film. Adapted from [36]

4.2.2 Coercivity of ferrite wood in a function of X ($Mn_xZn_{1-x}Fe_2O_4$)

The Coercivities of Mn-Zn ferrite wood was obtained from the hysteresis curve (figure 4.27). The coercivities were decreased by increased on Mn^{2+}. The different of coercivity occurred in parallel and perpendicular direction which is higher in perpendicular directions. The coercivities were lower compared with thin film but similar tendency was reveal.

Sorescu et al (2005)[29] stated that the Comparison of bulk and film magnetic properties shows that the magnetic properties of the films are in many respects similar to those of the bulk, which makes the laser ablation deposited ferrite films prime candidates for thin-film high-frequency microwave device applications. In particular, the saturation magnetization is very similar to the bulk value, but the coercivity values are slightly different.

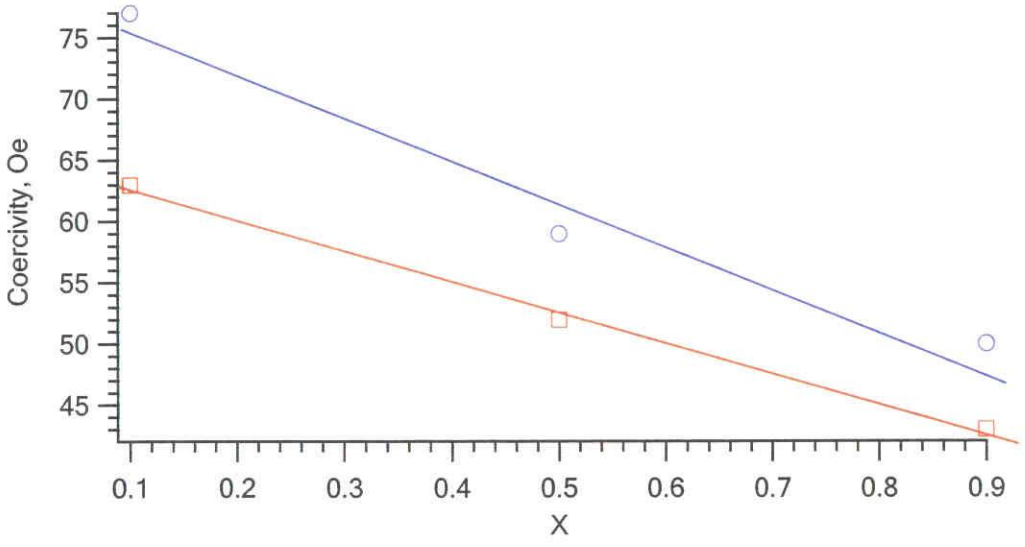

Figure 4.27 The coercivity of $Mn_xZn_{1-x}Fe_2O_4$ wood that measured parallel and perpendicular to the pores directions.

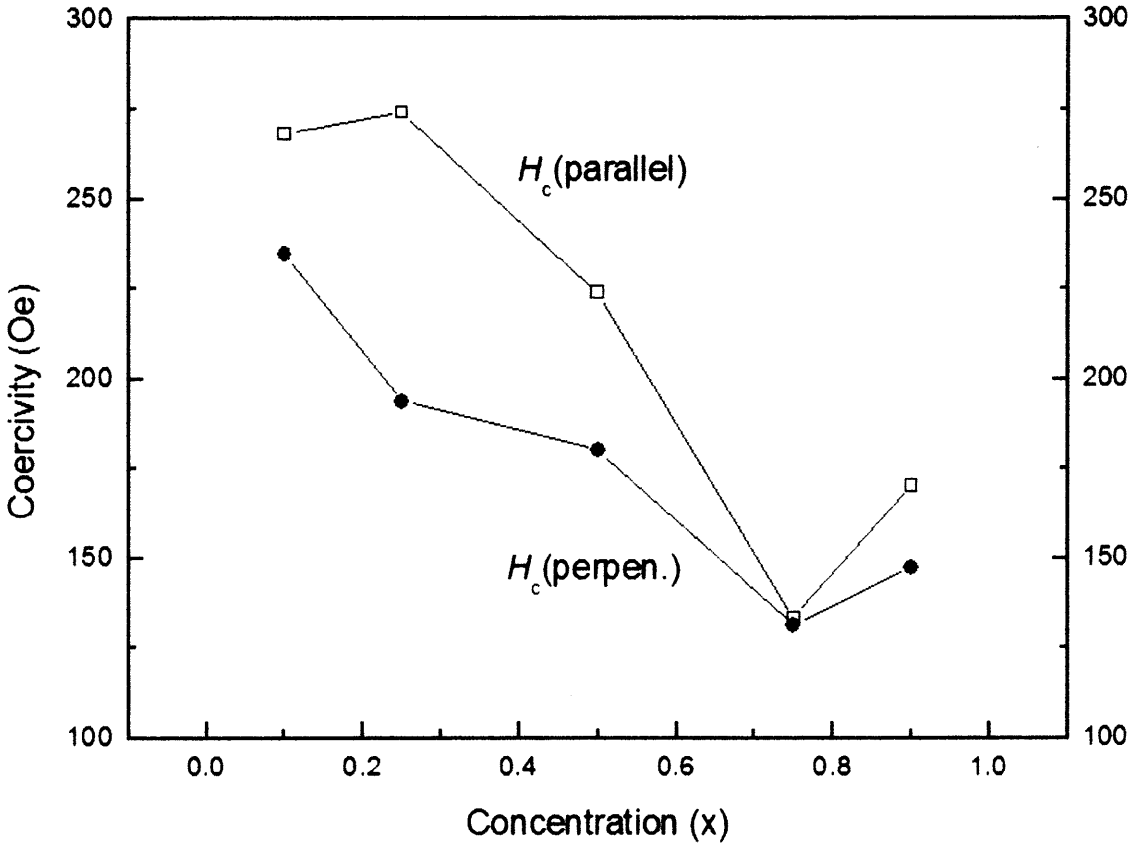

Figure 4.28 Variations of the coercivities (HC) of $Zn_{1-x}Mn_xFe_2O_4$ ferrite film under the parallel external field and the perpendicular external field. Adapted from [8]

4.2.3 Magnetic Saturations of Mn-Zn ferrite wood

Figure 4.29 shows the magnetic saturation of Mn-Zn ferrite wood. The magnetic saturations were increased by amount of Mn^{2+}. The magnetic saturations are 6 emu/g, 21 emu/g and 25.5 emu/g for amount of Mn^{2+}, x = 0.1, 0.5 and 0.9 respectively. The increments were corresponded with the net moment that calculated theoretically from outer-shell electron configuration and number of unpaired electron. The pattern of the normal spinel, mixed spinel and inverse spinel was increase constantly in straight line. The results show the increment able to retain at Mn^{2+} exceeded 50%.

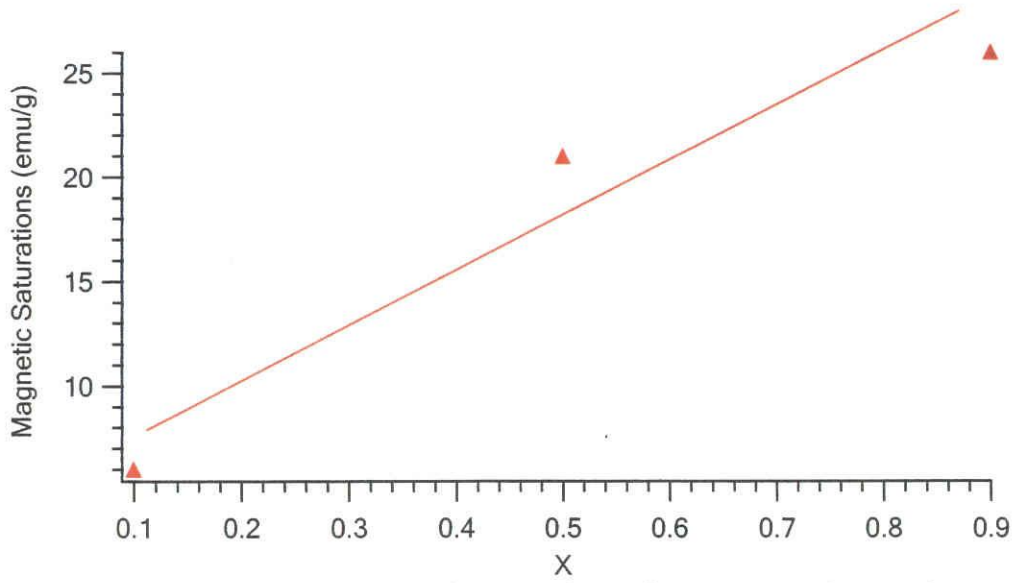

Figure 4.29 The magnetic saturations of $Mn_xZn_{1-x}Fe_2O_4$ wood

4.2.4 Saturation magnetization ratio (Squareness) of Mn-Zn ferrite wood

The squareness of Mn-Zn ferrite woods have a similar tendency with Ni-Zn ferrite which is the squearness were increase by decreasing of Zn^{2+}. But the different of parallel and perpendicular directions are smaller (average different 1%) (figure 4.30).

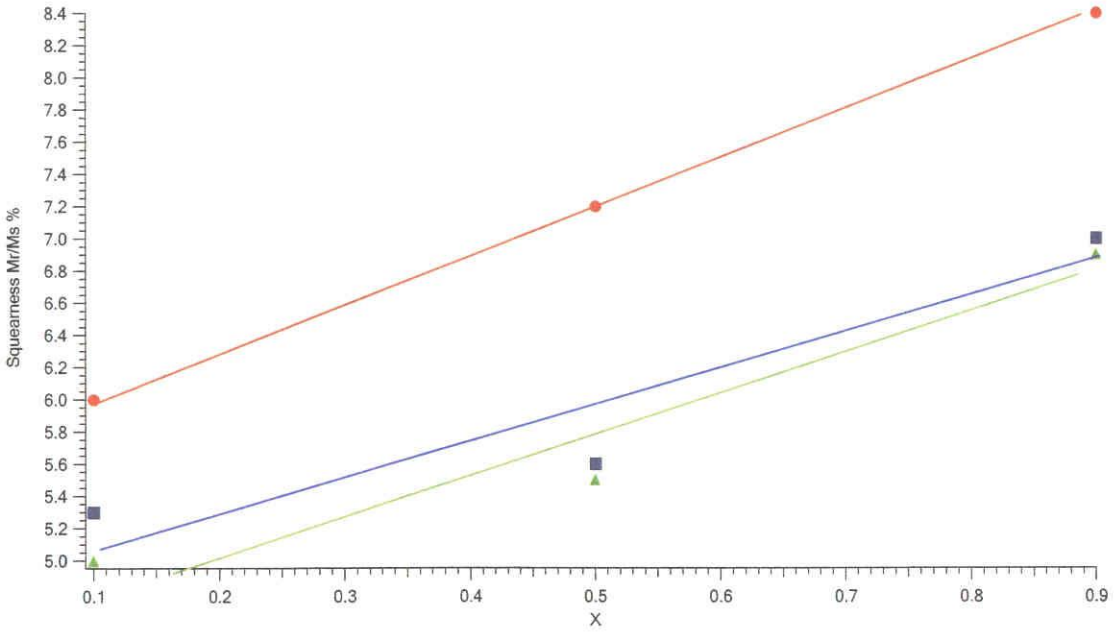

Figure 4.30 the squareness of $Mn_xZn_{1-x}Fe_2O_4$ Wood

4.2.5 Hysteresis curve of thinner $Mn_{0.5}Zn_{0.5}Fe_2O_4$ woods

Previously, the cubical shape specimens were measured and the anisotropy occurred due to the woody shape. The questions are… thus anisotropy will occurred in the different shape of specimens? Or it changes with the thickness of specimen? To answer thus question, the thin specimens were measured (≥1mm). Three different directions were examined by using VSM.

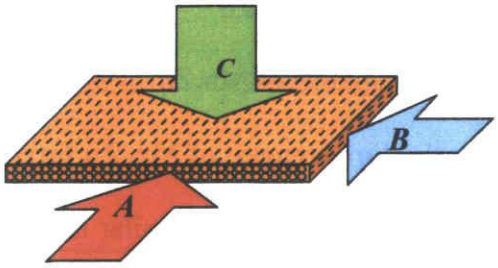

Figure 4.31 $Mn_{0.5}Zn_{0.5}Fe_2O_4$ wood in thin shape for VSM measurement

The figure 4.31 shows the magnetic hysteresis of the $Mn_{0.5}Zn_{0.5}Fe_2O_4$ wood that measured in A, B and C directions. The saturation of magnetization for C direction was lowers than A and B directions because of the demagnetizing effects associated with the thin/ short specimen.

But after normalized the curve in M/Ms (figure 4.32) the A direction that measured in parallel with the pores was easier to magnetize. Meanwhile for B and C direction seem identical. It has a similar tendency as cubical shape specimens. The magnetic saturations and the coercivity were similar with cubical shape specimens.

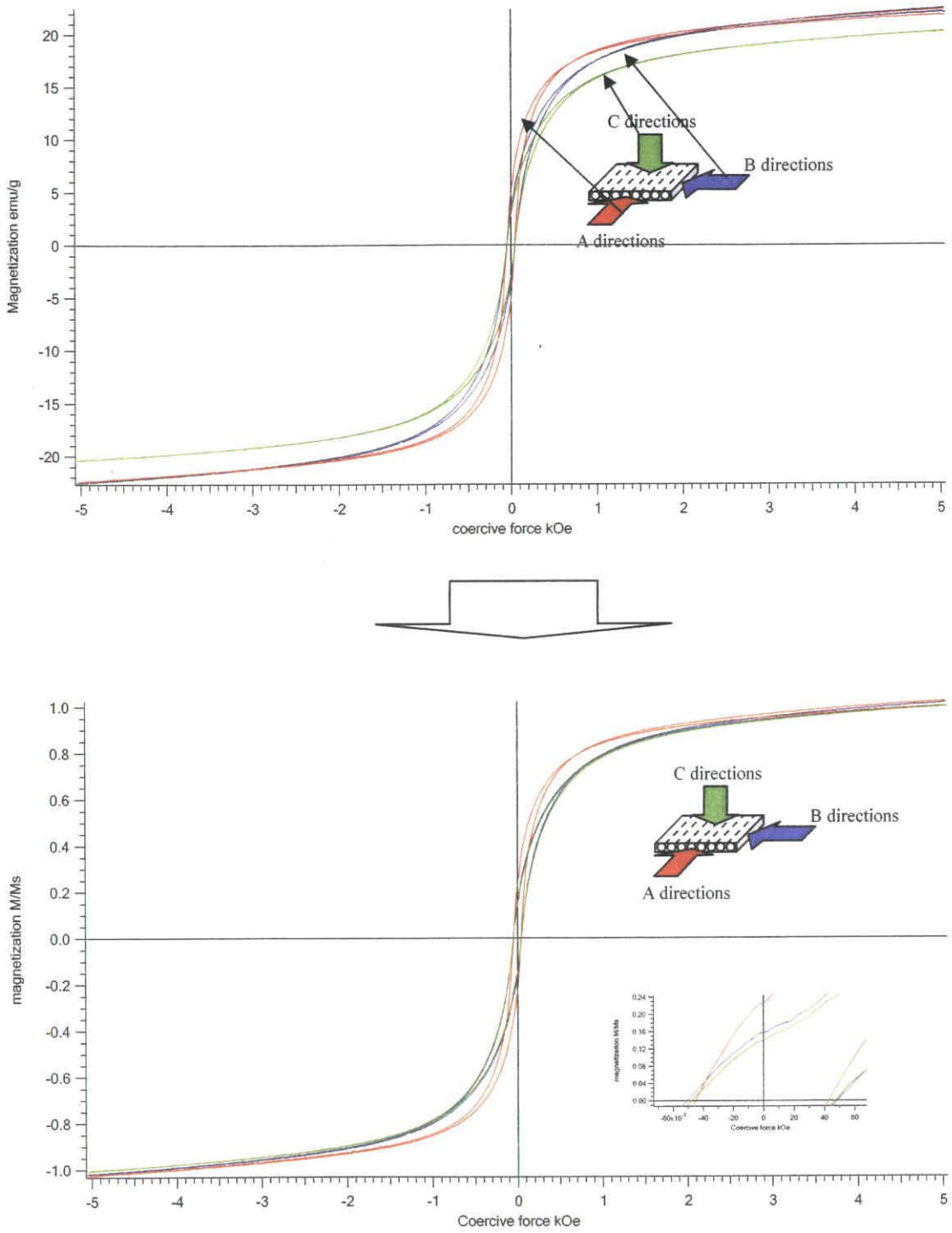

Figure 4.32 the normalized the curve in M/Ms of MnZn ferrite wood

4.2.6 Magnetic permeability of Mn-Zn ferrite wood.

According to [40] the permeability of typical ferrite family it shows that the Mn-Zn ferrite have a lowest effective frequency approximately 10 times lower than Ni-Zn ferrite. Because of this, the permeability of Mn-Zn ferrite was lower than air in

GHz frequency regions.

Figure 4.33 shows the magnetic permeability MnZn ferrite wood measured from 100MHz to 1Ghz, that From the results, we can conclude that Mn-Zn ferrite wood have a lower permeability at higher frequency regions.

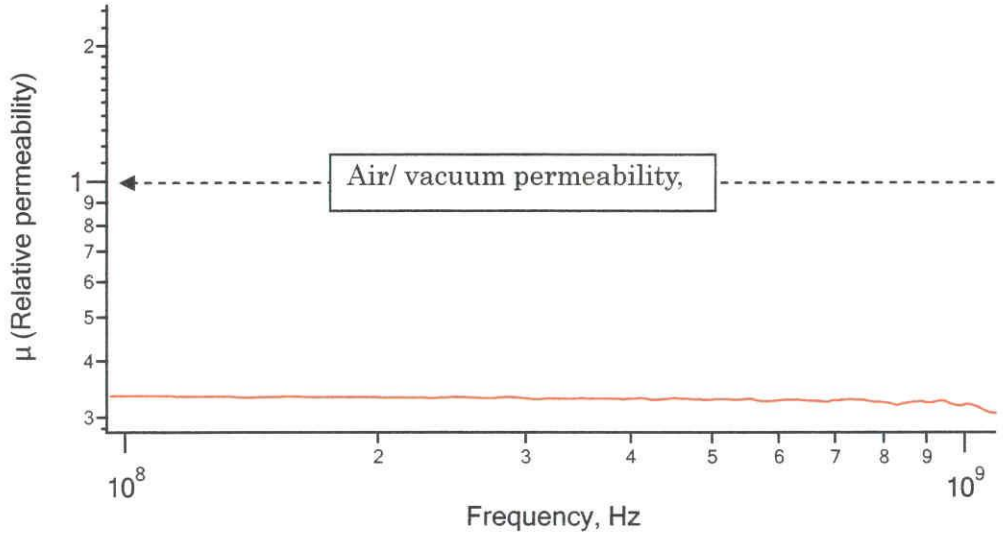

Figure 4.33 Permeability of $Mn_{0.5}Zn_{0.5}$ Ferrite at 100MHz – 1GHz

4.3 Magnetic properties of Ba-ferrite

4.3.1 Magnetic hysteresis of Ba- ferrite wood

In previous chapter described about the crystallization of Ba-ferrite and from the XRD pattern it shows that the α-Fe_2O_3 still retained at 1400°C. Sintered at 1400°C woody microstructure was completely deformed. And also single phase Ba-ferrite are crystallized at 1450°C [15,52] but the woody shape unable to retained at such high temperature due to the high shrinkages (figure 4.34).

At 1200°C the woody microstructure was only partially retained. The hysteresis loops of ba-ferrite are show in figure 4.35. It didn't indicate any specific trend affected by the wood microstructure. This might be because the woody microstructure that partially retained and the existing of α-Fe_2O_3.

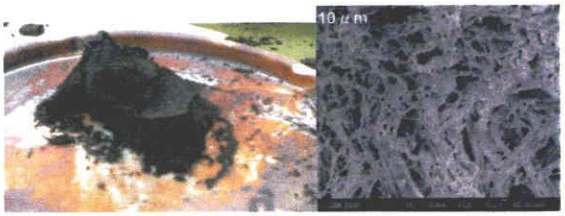

Figure 4.34 Photo and SEM image of Ba-ferrite wood sintered at 1200°C

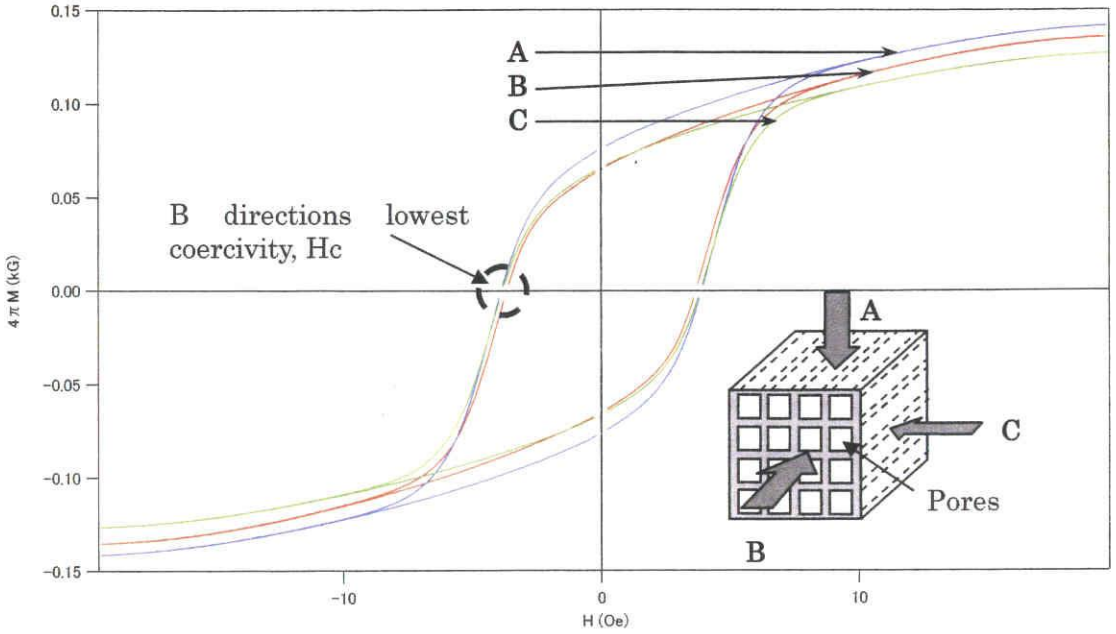

Figure 4.35 hysteresis loop of Ba-ferrite + hematite partially wood.

Compared with NiZn ferrite and MnZn ferrite that able to retain the woody microstructure at single phase, the easy axis of the hysteresis loops was easy to be identified. But for the Ba-ferrite wood + hematite the squareness are similar in all directions. Only the coercivity in B directions was slightly small. Probably due to the small number of the woody shape microstructure.

The partially Ba-ferrite woods didn't perform the hysteresis loop as Ba-ferrite film. This is because, the complete single phase Ba-ferrite can be obtained at high temperature (1450°C onward). Meanwhile the wood microstructure can't retain at such temperature.

4.3.2 Permeability of Ba-ferrite wood

Figure 4.37 shows the Ba-ferrite wood that sintered at 1000°C – 1400°C. The

result indicates the low bulk density Ba-ferrites have a small value of magnetic permeability. The specimens sintered at 800°C and 1000°C have a low permeability ~1 because of the low bulk density.

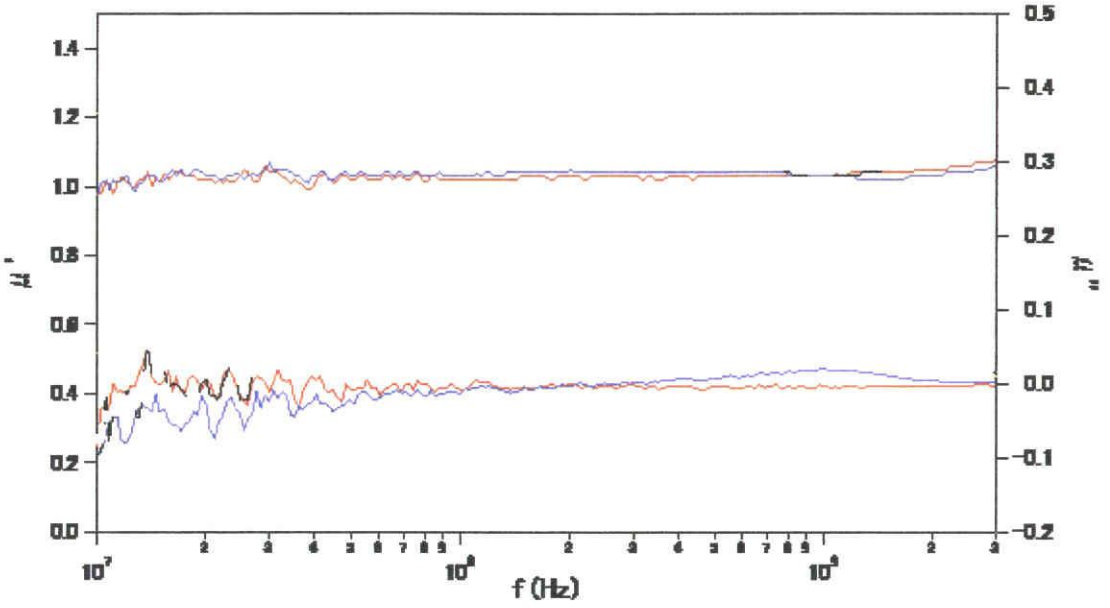

Figure 4.37 Permeability of Ba-ferrite wood sintered at various temperature (red) 800°C, (blue) 1000°C

4.4 Advantages of Ferrite wood

Ferrite woods have advantages due to the microstructures. The physical characteristic of ferrite woods are the 1 directional pores. The function of the pores is to separate the sintered body into thin layer that constructed by combinations of grains. Thus characteristics capable to influence the magnetic ability due to the arrangement of grains.

Due to the micro-size of the pores and thickness of the wall of sintered body, the woody shape can be retained as thin as 50μm or less and almost similar thickness as thick film.

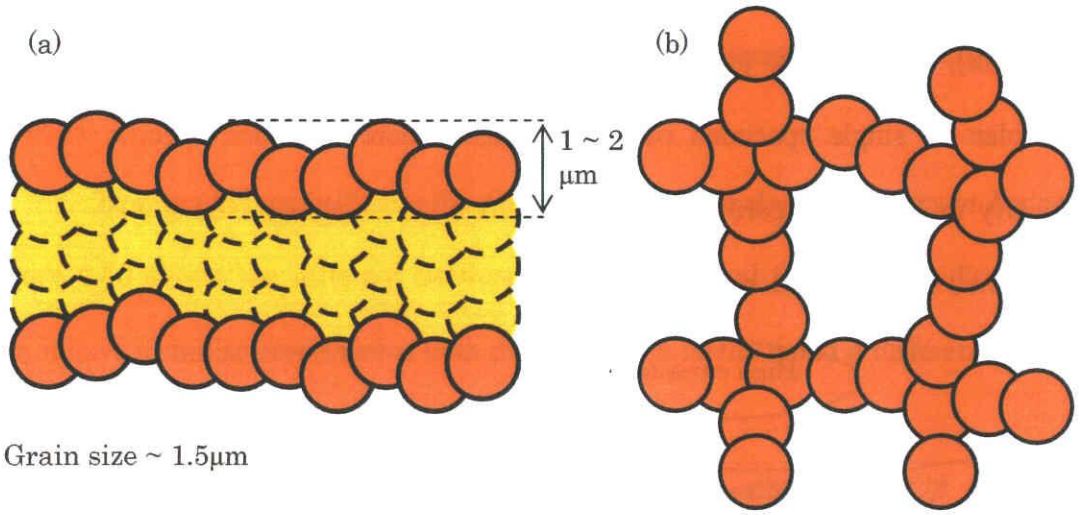

Figure 4.38 schematic of grain distribution (a) side view, (b) Front view

Film shape specimens have better magnetic properties because most of the measurement equipments were considers the volume of the specimens instead of mass.

Jianhua Gao et al. (2004)[42] that prepared results they prove that for thin film of $Ni_{0.4}Zn_{0.6}Fe_2O_4$ has a highest magnetic saturation (approximately 400emu/cc). They also mention that for bulk ferrite, the maximum magnetic saturation is occurred at 50% of Zn concentrations. The coercivity, Hc also increase monotonously by increasing of Nickel contains. The inclinations of Hc vs X (x= contain of Nickel) showed that in perpendicular direction of film have a higher coerciveity. The reason Ni-Zn ferrite film have a higher coercivity compared with bulk was discussed.

Beside that, the film shape specimen was constructed by a layer that arranged in the surface of the substrate. This geometry caused the existing of easy and hard axis which is in easy axis was easier to magnetize. In the case of Ni-Zn ferrite film, it has a higher squareness (ratio Mr/Ms) in easy axis [30] but have a higher coercivity at hard axis [42]. Both parameters are important to be high. But most of the application was limited to the in- plane directions (easy axis). Until now for mixed spinel ferrite, in-

plan directions have only limited to one specific magnetic property for single specimen (fig 4.38). I believe the potential usage of mixed spinel ferrite might be increase if 1 plan of single specimen of ferrite consist more than one specific magnetic property in 1 plane (figure 4.39). The additional advantages mixed spinel ferrites was obtained by woody microstructure.

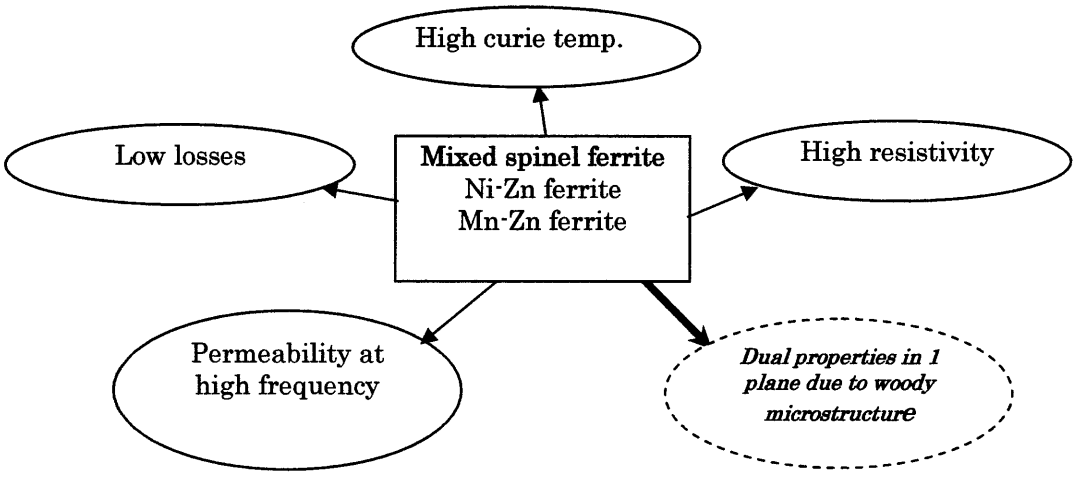

Figure 4.39 The advantages of mixed spinel ferrite

H.M.El-Sayed (2009) [45] have improved the Squareness (Mr/Ms) and the Hc due to the magnetic anisotropy of Co-ferrite (spinel ferrite) by inducing pressure and external magnetic field at the powder.

The multilayer films have a good potential to obtain such phenomenon. But it needs complicated and special equipment to produce it. We have found that the wood is a good candidate because it contained of elongated tubular cells aligned with the axis of the tree trunk [1]. The wall was separated by 1 directional pores. The behaviors of ferrimagnetism exist at the compounds which have more complex structure than element. For example, Ni-ZnFe_2O_4 and Mn-Zn Fe_2O_4 that only a portion of the ion contributes to the magnetization of the materials. Theoretically both Mn-Zn ferrite and Ni-Zn ferrite have a similar crystal structure (Mixed spinel ferrite). Thus ferrite woods have a woody microstructure. In term of magnetic properties, It have a anisotropy effect due the microstructure of wood if external field induced,

which are higher squareness in parallel with the wall. Sintered at 1200°C the thickness of wall was approximately 1-2μm. The squareness are increase by decreasing of Zn^{2+} contains.

The results was indicates the ferrite wood have a dual properties in 1 plane.

Figure 4.40 shows the different between ferrite wood and ferrite wood. For ferrite film it have a similar properties at both directions, but ferrite wood it different.

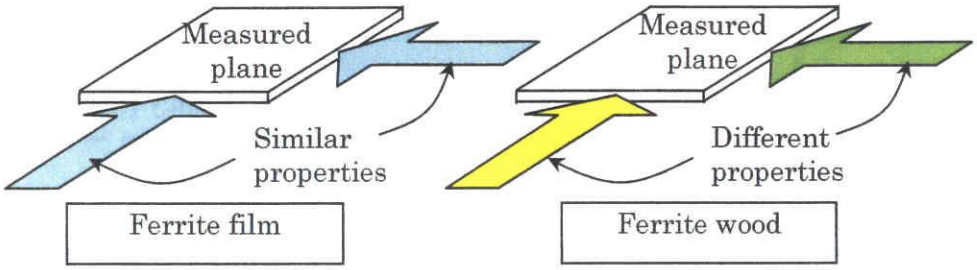

Figure 4.40 The different of ferrite film and ferrite wood

4.5 Comparison of NiZn-ferrite, MnZn-ferrite and Ba-ferrite wood.

Generally, NiZn-ferrite, MnZn-ferrite and Ba-ferrite are chemically different. NiZn-ferrite, MnZn-ferrite has a similar crystal structure but different especially in magnetic hysteresis due to the net moment of unpaired electron shell. The Magnetic moment of NiZn-ferrite is higher than Mn-Zn ferrite and Ba-ferrite. Theoretically solid Ba-ferrites have permeability ~10 at GHz region. But in the case of Ba-ferrite wood that have a very low bulk density, caused the permeability was lower (~1).

Among these 3 ferrite wood, Ni-Zn ferrite wood have a highest permeability at higher frequency. This is because,

- The NiZn ferrites have a high permeability at high frequency (max peak at 10 – 100 MHz).
- At low bulk density, the permeability is better at high frequency regions.

- The effects of woody microstructure (multi layer film) enhance the permeability at higher frequency region.

Meanwhile for MnZn ferrites, it has a low permeability at higher frequency because,

- The MnZn ferrites have a high permeability at low frequency (max peak at 500 kHz – 1 MHz).
- At low bulk density, the permeability is better but, at 10 - 100MHz the permeability was drop lower than 1.

For Ba-ferrite

- The Ba- ferrites have a high permeability at high frequency (max peak at 1 GHz).
- In high bulk density Ba-ferrite the permeability are low. That mean for low bulk density ferrite the permeability are lower.
- Ba-ferrite wood can't be produce in single phase. This is because the complete single phase only can be produce at >1400°C. The woody microstructure can't retain such high temperature.

Figure 4.41 shows the approximations permeability of solid ferrite and ferrite wood. The higher permeability at higher frequency region is the main focus in this study. NiZn ferrite wood is the best candidate among all.

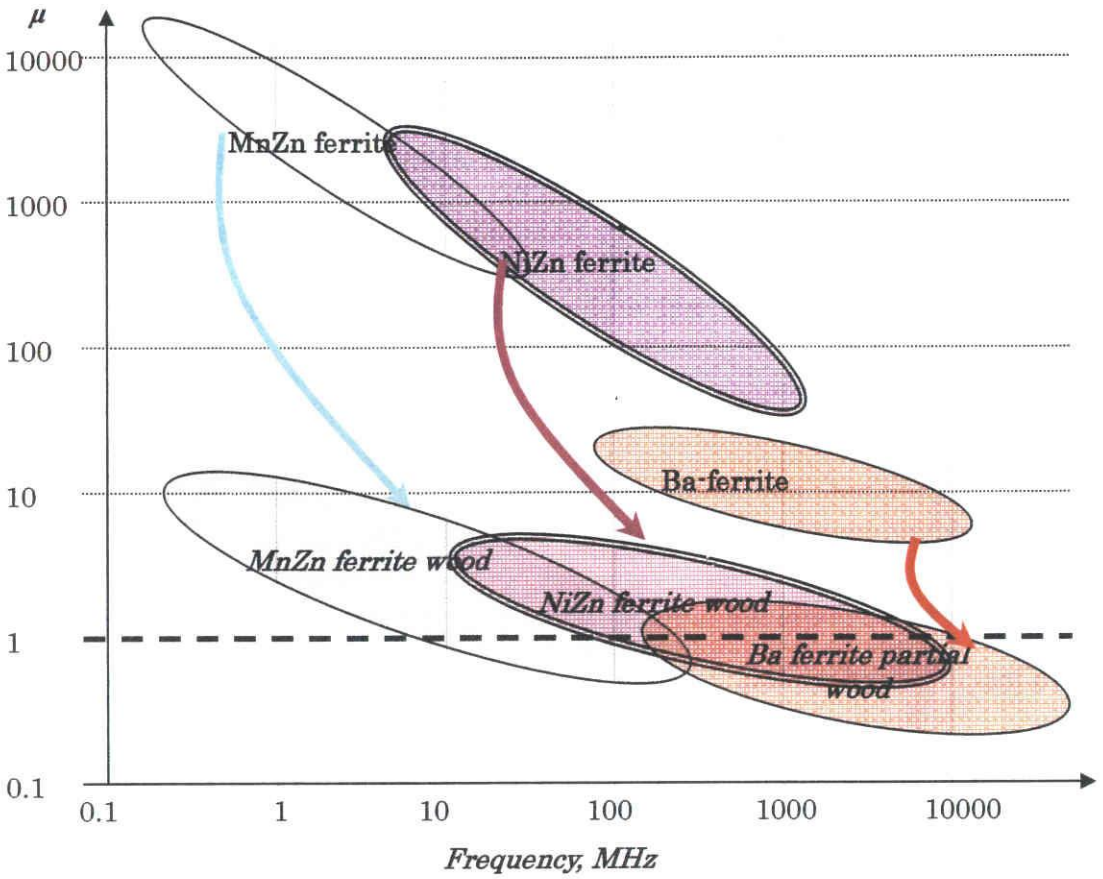

Figure 4.41 Approximations permeability of solid ferrite and ferrite wood

Because of this reason; the reflections loss of the NiZn ferrite was investigated. Ni-Zn ferrite is widely used as electromagnetic wave absorber in the VHF/UHF region. Many studies were carried out to investigate the microstructure of chemistry dependence of magnetic permeability for producing a well-controlled ferrite absorber [55-56]. The results revealed the different of the magnetic properties caused by the microstructure. The return loss of Ni-Zn ferrite was change by the volume fractions [57] composition [55, 58] and the thickness [55,59] of the specimens. Instead of that the number of the layer [57, 59] was also influenced.

The return loss was determined by the S parameter measured by 1 port coaxial cable. The equations of return loss or reflections loss (RL) are show below.

$$RL = 20 \log_{10} S_{11} \quad \text{.....} \quad (4.1)$$

Which is S_{11} is the input port voltage reflection coefficient. The S-parameter for a 1-port network is given by a simple 1 x 1 matrix of the form (S_{nn}) where n is the allocated port number. To comply with the S-parameter definition of linearity, this would normally be a passive load of some type. The measured S parameter was in Complex form that involving the real and imaginary parts that shown in equation below.

$$S_{11}^2 = S_{11r}^2 + S_{11i}^2 \quad \text{..... (4.2)}$$

By substituting the equation (4.2) into (4.1) we get

$$\text{Return loss, } RL = 10 \log_{10} (S_{11r}^2 + S_{11i}^2) \quad \text{..... (4.3)}$$

4.6 Return loss / Reflections loss

Figure 4.42 shows the results of the returns / reflections loss of $Ni_{0.5}Zn_{0.5}Fe_2O_4$ in different microstructure. All the measured specimens were subjected with the similar composition and bulk density. For each set of specimens, the obtained return loss result slightly different due to the un-uniform of the pores sizes.

But the produce- able results for each set specimens were with in certain frequency ranges. The results show that the vertical pore ferrite woods have the highest frequency peak at 4 – 6 GHz. Meanwhile for horizontal pores ferrite wood the peaks range was around 2 - 3 GHz. The non-wood microstructure specimen has a lowest frequency range which is lower than 1 GHz. The results were corresponded with the magnetic permeability of the specimens. In sections was discussed the permeability of the specimens. The vertical pores ferrite wood specimens have a highest permeability at the GHz region follow by the horizontal ferrite wood specimens finally non- wood microstructure ferrite specimens.

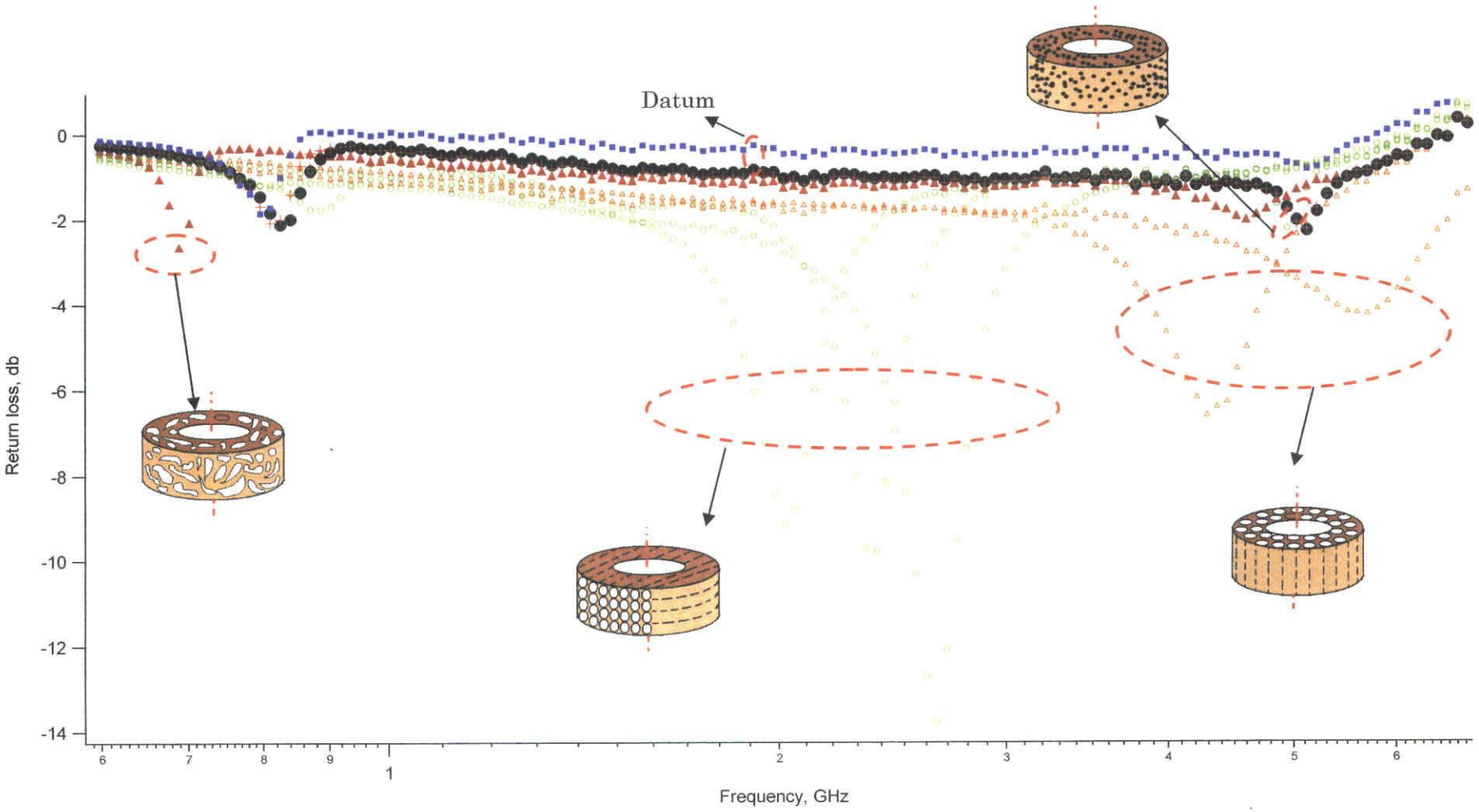

Figure 4.42 The return loss, RL (db) Vs frequency, GHz of the ferrite wood and low density Ni-Zn ferrite

CHAPTER 5

CONCLUSIONS

5.1 Conclusions

The aims of this study if to develop the mixed spinel ferrites (Ni-Zn ferrite and Mn-Zn ferrite) and hexagonal ferrite (ba-ferrite) by using wood templates and determine the magnetic properties of thus novel microstructure that different between bulk conditions. This thesis is contribute to the new condition of microstructures that consisted the systematic array of the pores that mimicking wood templates. In the other hand, due to the condition of thus microstructure was contributing to the new phenomena of magnetic properties that similar tendency as film shape.

The optimum preparation condition of Ni-Zn ferrite and Mn-Zn ferrite from wood template was successfully obtained. The crystallizations of single phase ferrite were determined by controlling the sintering temperatures, times and atmosphere. The different preparation conditions were revealed between thus soft ferrites. As a results thus ferrite wood was successfully prepared with a minimum defects.

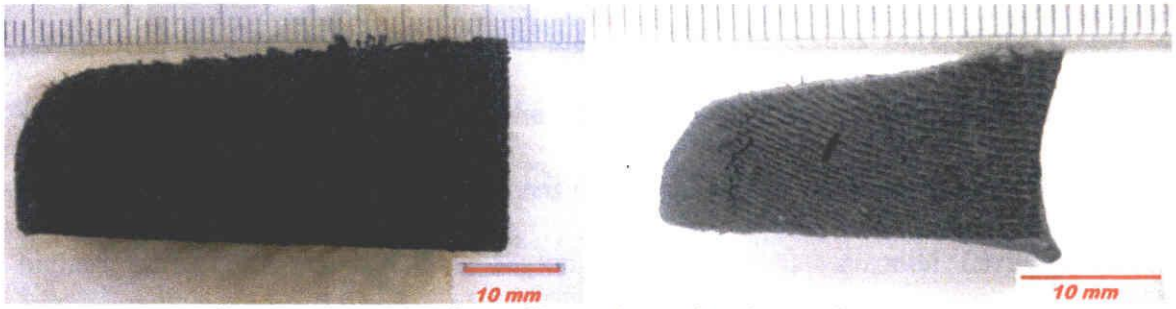

Figure 5.1 Image of a. Infiltrated template b. Ferrite wood

The magnetic hysteresis (B-H curve) of ferrite wood in cubical shape was presented. Normally for soft ferrite, in bulk conditions the hysteresis is isotropic in any

direction that measured with the same thickness. But for ferrite wood even tough the physical appearances look like bulk ferrite, but the magnetic hysteresis anisotropy was revealed (easy axis and hard axis). This phenomenon similar with the film shape ferrite because ferrite wood are reacting like multilayered ferrite film. Figure 5.2 indicated the advantages of Spinel ferrite wood. The Dual magnetic property due to woody microstructure was revealed.

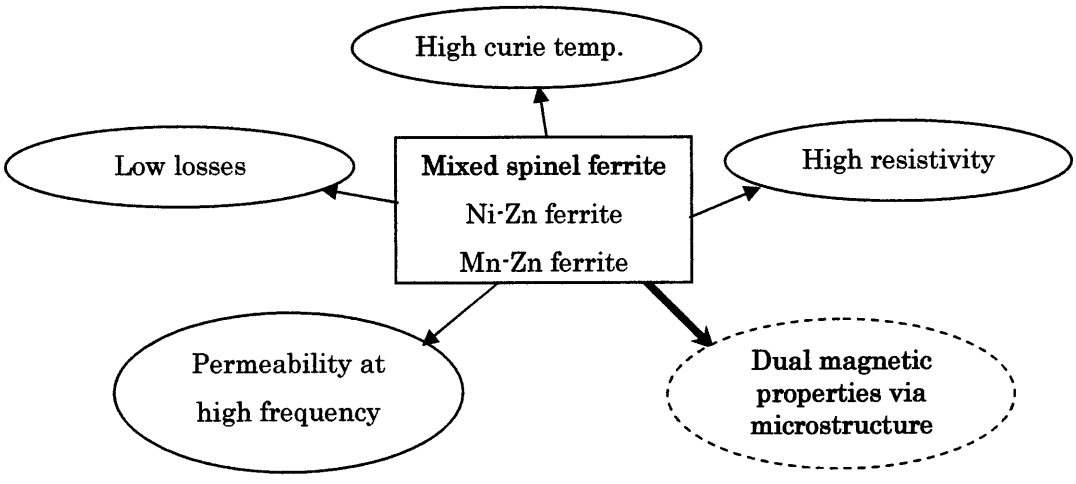

Figure 5.2 the advantages of ferrite wood

The microwave properties were studied. The magnetic permeability, μ was investigated. Due to the microstructure of ferrite that mimicking the wood, we had revealed the permeability, μ was higher when the layer of wall of ferrite wood measured parallel with the magnetic field, B.

Among thus 3 ferrite woods, NiZn ferrite wood have better performance at higher frequency region. Because of that reason, the Reflection Loss, RL of NiZn ferrite wood was investigated. As results, the Reflection Loss of NiZn ferrite wood shows the effective frequency range at GHZ regions. The specimens NiZn ferrite wood that the pores that arrange vertically have zero reflections loss at frequency range around 4-6GHz. For the non- woody microstructure have the zero reflections loss frequency

lower than 1GHz. The NiZn ferrite wood that constructed from multilayer wall able to shifted the zero reflections loss to higher frequency regions.

5.2 Suggestions for future study

For the future study, I suggest investigating reflection loss due to relationship between permittivity, ε and the permeability μ of this ferrite wood and related it with the theory. Instead of that the absorptions loss of ferrite wood is also suggested for the future study.

REFERENCES

[1] P.Greil. *Journal of the European Ceramic Society 21 92001) 105-118*

[2] Zhaoting Liu, Tongxian Fan, Wang Zhang and Di Zhang. *Microporous and Mesoporous Materials 85 (2005) 82-88.*

[3] Andre R. Studart, Urs T. Gonzenbach, Elena Tervoort and Ludwig J. Gauckler, *Journal American Ceramic Society 89 [6] 1771-1789 (2006)*

[4] T.Ota, M. Imaeda, H. Takase, M. Kobayashi, N. kinoshita, T. Hirashita, H. Miyazaki, Y. Hikichi, *Journal American Ceramic Society 83 (2000) 1521-1523.*

[5] T.Hirashita, H.Miyazaki, H. Takase, N. Kinoshita, T.Ota, *Ceramic Transactions 112 (2001) 521-526.*

[6] D. Mallick, O.P. Chakrabarti, H.S. Maiti and R. Majumdar, *Ceramic International 33 (2007) 1217-1222*

[7] Teresa L. Y. Cheung and Dickon H.L. Ng, *Journal American Ceramic Society, 90 [2] 559 – 564*

[8] T. Ota, Minoru Takahashi, Toshiyuki Hibi, Masakuni Ozawa, Suguru Suzuki and Yasuo Hikichi. *Journal American Ceramic Society, 78 [12] 3409 – 11 (1995)*

[9] Y. Matsumura, I. Kamada, T.Shiono, T.Nishida, *J. Soc. Mat. Sci. Jpn 52 (2003) 576-580*

[10] E. Vogli, J. Mukerji, C. Hoffman, R. Kladny, H. Sieber, P. Greil, *Journal American Ceramic Society 84 (2001) 1236 – 1240.*

[11] Carlos Renato Rambo, Tarcisio Andrade, Tobias Fey, Heino Sieber, Antonio Eduardo Martinelly and Peter Greil, *Journal American Ceramic Society, 91 [3]*

852-859 (2008)

[12] Mamoru Mizutani, Haruyuki Takase, Nobuyasu Adachi, Toshitaka Ota, Keiji Daimon, Yasuo Hikichi, *Science and Technology of Advance Materials 6 (2005) 76-83.*

[13] Zhaoting Liu, Tongxiang Fan, Wang Zhang, Di Zhang, *Microporous and Mesoporous Materials 85 (2005) 82-88*

[14] K.H.Wu, Y.M.Shin, C.C. Yang, G.P. Wang and D.N.Horng, *Materials Letters 60 (2006) 2707-2710*

[15] Lanlin Zhang, Ferrites for UHF applications, *Inorganic Material Science The Ohio State University, June 2006.*

[16] J.Smit and H.P.J.Wijn, Ferrites, *International version 1959 Philips Tech Lib and Tokyo Electrical Engineering College press, Japan U.D.C. Nr. 538.221:621.318.124*

[17] S.Deka, P.A. Joy, *Materials Chemistry and Physics 100 (2006) 98- 101.*

[18] Seema Prasad, N.S. Gajbhiye, *Journal of Alloys and Coumpounds 265 (1998) 87-92.*

[19] A. Thakur, M.Singh, *Ceramic International 29 (2003) 505-511*

[20] Kenneth L. Kaiser, *Electromagnetic Shielding, 2006 Taylor & Francis Group*

[21] Jianhua Gao, Yitao Cui, Zheng Yang, *Materials Science and Engineering B 110 (2004) 111-114.*

[22] D. Ravinder, K. Vijay Kumar, A.V. Ramana Reddy, *Materials Letters 57 (2003) 4162–4164*

[23] B. Parvatheeswara Rao, A. Mahesh Kumar, K. H. Rao, Y. L. N. Murthy, O. F. Caltun, *Journal Of Optoelectronics And Advanced Materials Vol. 8, No. 5,*

(October 2006), 1703 -1705

[24] Zhifeng Zhong, Qiang Li, Yiling Zhang, Haisheng Zhong, Ming Cheng, Yang Zhang, *Powder Technology 155 (2005) 193 – 195.*

[25] J. Azadmanjiri, *Materials Chemistry and Physics 109 (2008) 109–112*

[26] A. Verma, T.C. Goel, R.G. Mendiratta, R.G. Gupta, *Journal of Magnetism and Magnetic materials 192 (1999) 271-276.*

[27] Chien-Yih Tsay, Kuo-Shung Liu, I-Nan Lin, *Journal of the European Ceramic Society 21 (2001) 1937-1940.*

[28] Purushotham Yadoji , Ramesh Peelamedu, Dinesh Agrawal, Rustum Roy, *Materials Science and Engineering B98 (2003) 269_ 278*

[29] Monica Sorescu, L. Diamandescu, R. Swaminathan, M. E. McHenry, M. Feder, *Journal of Applied Physics* ***97****, (2005), 10G105*

[30] O. F. Caltun, *Journal of Optoelectronics and Advanced Materials Vol. 7, No.*

[31] J.C. Andason, K.D. Leaver, R.D. Ranlings and J.M. Alexander *"Material Science" 4th Ed. Champan and Hall, 11 New Fetter Lane London, (1990)*

[32] J.Bera et all (2005)

[33] S. M. Attia, *Egypt. J. Solids, Vol. (29), No. (2), (2006)*

[34] Manual and Principle measurement PMF- 3000 Ryowa

[35] H.M. El-Sayed, *Journal of Alloys and Compounds 474 (2009) 561-564*

[36] R.G. Welch, J. Neamtu, M.S. Rogalski, S.B. Palmer, *Material letter 29 (1996) 199- 203*

[37] M. Jalaly, M.H. Enayati, F. Karimzadeh, *Journal of Alloy and Compound (2009) in press*

[38] P. Ravindranathan, K.C. Patil, *Journal of Materials science 22 (1987) 3261-3264.*

[39] H.su et al (2007)

[40] Jorg Topfer, Julia Murbe, Andre Angermann, and Silvia Kracunovska, Stefan Barth, Franz Bechtold, *Int. J. Appl. Ceram. Technol., 3 [6] (2006) 455–462*

[41] Muhammad Ajmal, Asghari Magsood, *Materials letters 62 (2008) 2077-2080*

[42] Jianhua Gao, Yitao Cui, Zheng Yang, *Materials Science and Engineering B 110 (2004) 111-114*

[43] C.Calle, et al. *Physica B 384 (2006) 103 – 105*

[44] W.D. kingery, H.K.Bowen, D.R Uhlmann, *Introduction to ceramic 2nd ed. A Willey-Interscience Publication.*

[45] H.M. El-Sayed, *Journal of Alloys and Compounds 474 (2009) 561-564*

[46] M.I. Rosales, M.P. Cuautle, V.M. Castano, *J. Mater. Sci* 33, 3665(1998).

[47] E.Schloemann et al. *IEEE Transactions on Magnetics,* 31 [6] 3470-3472(1995).

[48] Jae- Guang Lee et al, *Journal of the Korean Physical Society, Vol [**49**], No 2, August 2006, pp. 604 – 607*

[49] S.M. Attia, *Egypt. J. Solids, Vol. [**29**], 2006, No. (2).*

[50] N.Spaldin, Magnetic Material and device applications, *Cambridge university press, 2003*

[51] Xiao-Hui Wang, Tian-Ling Ren, Long-Yu Li and Lian-Sheng Zhang, *Journal of Magnetism and Magnetic Materials 184 (1998) 95-100.*

[52] G. Winkler, "*Crystallography, chemistry and technology of ferrite" in Magnetic properties of material ed J. smith, NY, McGraw-Hill, 1971.*

[53] Jianxun Qiu, Mingyuan Gu, *Journal of alloys and Compounds 415 (2006) 209-212.*

[54] Wen-tsang Liu, Jenn-Ming Wu, *Materials Chemistry and Physics 69 (2001) 148- 153.*

[55] Sung-Soo Kim, Dae-Hee Han, *IEEE Transactions on Magnetic, Vol 30, No6 Nov 1994*

[56] H.T.Hahn, *Journal Applied Physic, Vol 69 pp 6192-6194, 1991*

[57] Dong-Young Kim and Yeon-Choon Chung, *IEEE Transactions of electromagnetic Compatibility Vol 3, No 4, 1997*

[58] Yeon Hwang, *Materials letters 60 (2006) 3277-3280*

[59] Hiroki Anzai, Yoshiyuki Naito, Tetsuya Mizumoto, *Tokyo Institute of Technology.*

[60] Hao Tang, Wenxu Zhang , Bin Peng, Wanli Zhang *Thin Solid Films 518 (2010) 3342–3344*

[61] Hideo Oka, IEEJ Transactions on fundamentals and Materials vol.126 (2006), No1 pp.22-27

[62] Hideo Oka, A.Hojo, H. Osada, Y. Namizaki and H. Taniuchi, J.Magnetism & Magnetic Materials, Vol. 272-276

[63] H. Oka andH. Fujita. J. Appl. Phys., Vol 85, No.8 Part 2,15, pp 5732-5734 (1999)

[64] H. Oka, K. Narita, H. Osada and K.Seki., J. App. Phys., Vol 91, No10, pp 7008-7010 (2001)

ACKNOWLEDGMENT

At first thanks to the God, that leads the way for the success of this study.

I would like to express my appreciations to my supervisor Professor Dr Toshitaka Ota for his guidance, valuable suggestions, and elaborate discussions and also helps me on my living in Japan. And also Assoc. Prof. Dr Nobuyasu Adachi that help me a lot in experimental, and theoretical and also Professor Dr Manabu Gomi from Department of Materials Science and Engineering, Nagoya Institute of Technology that contribute to the valuable comment and suggestions. This study would not survive without your guidance and kind help. And for those who contributed in one way or another especially all the members of Ota's laboratory (next page).

Other than gaining knowledge in frontier material, I also learn a lot about the Japanese technology, hardworking culture, sincere people and delicious food. It is really an eye opening and exciting experience for me. Therefore, I want to express my gratitude to all those who have helped and contributed in one way or another during my stay in Japan.

And also, thanks to my whole family include my parents my brothers' and sisters' and also my wife and my children, that keeps on supporting and continually prays for me.

Finally, to Malaysian Government and Universiti Tun Hussein Onn Malaysia, who was granted and provided me the scholarship for this study. ありがとうございました。(Thank you very much)

Sia Chee Kiong

2011

Members of Ota's Laboratory (2008 – 2010)

2008

2009

2010

End of 2010